

Coarse-grained density functional theories for metallic alloys: Generalized coherent-potential approximations and charge-excess functional theory

Ezio Bruno,* Francesco Mammano, Antonino Fiorino, and Emanuela V. Morabito

Dipartimento di Fisica, Università di Messina, Salita Sperone 31, 98166 Messina, Italy

(Received 2 August 2007; revised manuscript received 10 January 2008; published 7 April 2008)

The class of the generalized coherent-potential approximations (GCPAs) to the density functional theory (DFT) is introduced within the multiple scattering theory formalism with the aim of dealing with ordered or disordered metallic alloys. All GCPA theories are based on a common ansatz for the kinetic part of the Hohenberg–Kohn functional and each theory of the class is specified by an external model concerning the potential reconstruction. Most existing DFT implementations of CPA-based theories belong to the GCPA class. The analysis of the formal properties of the density functional defined by GCPA theories shows that it consists of marginally coupled local contributions. Furthermore, it is shown that the GCPA functional does not depend on the details of the charge density and that it can be exactly rewritten as a function of the appropriate charge multipole moments to be associated with each lattice site. A general procedure based on the integration of the qV laws is described that allows for the explicit construction of the same function. The coarse-grained nature of the GCPA density functional implies a great deal of computational advantages and is connected with the $O(N)$ scalability of GCPA algorithms. Moreover, it is shown that a convenient truncated series expansion of the GCPA functional leads to the charge-excess functional (CEF) theory [E. Bruno *et al.*, Phys. Rev. Lett. **91**, 166401 (2003)], which here is offered in a generalized version that includes multipolar interactions. CEF and the GCPA numerical results are compared with status of art linearized augmented plane wave (LAPW) full-potential density functional calculations for 62 bcc- and fcc-based ordered CuZn alloys, in all the range of concentrations. Two facts clearly emerge from these extensive tests. In the first place, the discrepancies between GCPA and CEF results are always within the numerical accuracy of the calculations, both for the site charges and the total energies. In the second place, the GCPA (or the CEF) is able to very carefully reproduce the LAPW site charges and a good agreement is obtained also about the total energies.

DOI: [10.1103/PhysRevB.77.155108](https://doi.org/10.1103/PhysRevB.77.155108)

PACS number(s): 31.15.E-, 71.55.Ak, 71.23.-k, 71.15.Nc

I. INTRODUCTION

After 40 years of studies and applications, it is now clear that the density functional theory (DFT)^{1,2} constitutes a formidable tool for the understanding of the matter. Nowadays, DFT-based total energy calculations^{3–6} and Car–Parrinello molecular dynamics simulations⁷ are used in a growing number of scientific fields, ranging from physics to chemistry to biology. The reason of such a ubiquitous fortune is that these methods are *ab initio*, in the sense that the only underlying models are the fundamental interaction laws and quantum mechanics. However, just because of their *ab initio* nature, DFT-based methods generally require large computational resources. In spite of the availability of faster and faster computers, this circumstance sets up the limitations to the applicability of the same methods.

Most DFT implementations are based on the Kohn–Sham scheme⁸ and require the solution for the wave functions of the appropriate Kohn–Sham Schrödinger equation. This usually implies the orthogonalization or the inversion of large matrices and, hence, a number of operations scaling, in principle, as N^3 , where N is the number of atoms in the system. While for semiconductors or insulators, the wave-function localization quite naturally leads to sparse problems, the case of metals appears to be the most challenging. For metallic systems, in fact, the computational effort required by wave-function-based approaches remains $O(N^3)$. Nevertheless, even for metals, approaches based on the direct minimization of the Hohenberg–Kohn functional with respect to the charge

density^{9–11} could achieve $O(N)$ scaling. In this case, the basic strategy consists in partitioning the system under consideration in a collection of weakly interacting fragments.^{12,13} Even with present day computers, the scaling properties of DFT algorithms with respect to the size of the system remain a crucial issue since they determine which classes of phenomena can be studied by *ab initio* methods.

Among DFT implementations, the oldest methods using such a *divide and conquer* strategy for metallic systems are perhaps the self-consistent versions of the Korringa,¹⁴ and Kohn and Rostoker¹⁵ multiple scattering theory (MST). The MST method⁶ views the system under consideration as a collection of fragments (usually in a one to one correspondence to lattice sites), whose scattering properties are determined by solving a Kohn–Sham Schrödinger equation. Once the fragment (or single site) scattering matrices are determined, they are assembled together with the free electron propagator in order to obtain the scattering matrix or, equivalently, the Green’s function of the system. Both the determination of the fragment scattering matrices and the potential reconstruction are $O(N)$, while, in principle, the solution for the global scattering matrix is an $O(N^3)$ problem, as it corresponds to the determination of the appropriate boundary conditions for the wave function in each fragment. However, a number of algorithms have been devised^{16–18} that are able to obtain $O(N)$ scaling by mapping the determination of the system’s Green function in a sparse problem. This is usually obtained by assuming zero the electronic propagator outside the so-called local interaction zone (LIZ) of each fragment. If

the free electron propagator is used, about ten neighbor shells should be included in the LIZ,¹⁶ while using screened propagators¹⁹ allows us to have much smaller LIZs: typically one or two neighbors shells¹⁷ are sufficient. Another remarkable feature of the MST method is that, being based on Green functions rather than on wave functions, it can easily deal with disordered systems and ensemble statistical averages. For this reason, since many years, the coherent-potential approximation (CPA) theory²⁰ for disordered alloys has been used in conjunction with the MST²¹ and the DFT.²²

The present paper shall be concerned with the study of metallic alloys in which the nuclei are assumed to occupy the positions of an ordered lattice, while substitutional disorder may be permitted. For these systems, in spite of the apparent complexity of the DFT algorithmic implementations, the analysis of large supercell calculations has allowed for the identification of remarkably simple trends. Namely, the charge excesses associated with each lattice site appear to be linear functions of the electrostatic potentials at the same site.^{23,24} These simple relationships, to be referred in the following as the qV laws, allow us to describe the “atoms” of each chemical species in an extended metallic system in terms of two parameters, say, the slope and the intercept of the above linear functions,^{25,26} and appear to be the appropriate generalization of Pauling’s concept of electronegativity²⁷ to solid state physics. We have already suggested that the qV laws can lead to important simplifications for total energy calculations in metallic alloys.²⁶ In the present paper, we shall introduce the class of the generalized CPAs (GCPAs) for dealing both with ordered and disordered metallic alloys. From the computational point of view, GCPA schemes present $O(N)$ scaling. Their principal virtue, however, is that, as we shall demonstrate, the GCPA functional *exactly* reduces to a *function* of the relevant charge multipole moments at the various lattice sites, thus constituting a *coarse-grained* approximate version of the original DFT. At a further level of approximation, the GCPA density functional leads to a Ginzburg–Landau functional, the charge-excess functional (CEF),²⁶ which is equivalent to the above linear qV laws and computationally inexpensive. The predictions of the GCPA and the CEF about the qV laws and total energies shall be compared vs full-potential linearized augmented plane wave (LAPW) calculations^{28,29} for 62 ordered crystal structures.^{30,31} Our conclusions shall be that, at least for the systems considered, both GCPA and CEF are generally able to correctly find out the system ground state and to fairly well reproduce the energy differences between ordered structures in a fixed concentration ensemble.

The paper is organized as follows. In Sec. II, we shall briefly review the MST version of the DFT. In order to have a functional form as much localized as possible, the relevant electrostatic contributions shall be rewritten by using an exact multipole expansion. In Sec. III, we shall introduce the class of the GCPA theories and investigate the analytical properties of the corresponding approximate density functional. Moreover, we shall obtain, as a further approximation to the GCPA, the CEF theory, already obtained in a much more phenomenological context,²⁶ which is offered here in a generalized form suitable for the inclusion of dipole or quadrupole interactions. In Sec. IV, we shall compare the numeri-

cal results obtained from the GCPA and CEF approximations with those from full-potential LAPW calculations. CEF and GCPA calculations appear *numerically indistinguishable*. Both theories are able to fairly well reproduce the LAPW total energies. In Sec. V, we shall draw our conclusions, make our comments, and briefly discuss the possible developments of CEF and GCPA theories.

II. REVIEW OF THE DENSITY FUNCTIONAL MULTIPLE SCATTERING THEORY

A. Multiple scattering theory formalism

In this subsection, we shall briefly overview the grand canonical ensemble formulation of the MST-DFT.^{2,5} Our aim shall be to develop a common ground for dealing both with ordered and substitutionally disordered systems. Although finite temperature, relativistic and magnetic generalizations could straightforwardly be carried out,⁵ in this paper, we focus on the nonrelativistic non-spin-polarized case at $T=0$. Furthermore, when not otherwise stated, we shall consider the local density approximation (LDA)⁵ to the DFT and assume to have ions of charge $+eZ_i$ fixed at the lattice positions \mathbf{R}_i .

In our discussion, the relevant density functional is the electronic grand potential^{22,32}

$$\Omega(T=0, V, \mu) = E_{tot} - \mu N(\mu) = - \int_{-\infty}^{\mu} d\varepsilon N(\varepsilon; \mu) + \int_{-\infty}^{\mu} d\mu' \int_{-\infty}^{\mu'} d\varepsilon \frac{dN(\varepsilon; \mu')}{d\mu'} + \frac{e^2}{2} \sum_{i,j(i \neq j)} \frac{Z_i Z_j}{R_{ij}}, \quad (1)$$

where V is the volume of the system, μ is the chemical potential, and E_{tot} is the sum of the total electronic energy and the nuclei electrostatic interaction. $N(\varepsilon; \mu)$ is the integrated density of states, which is related to the electronic density of states (DOS), $n(\varepsilon, \mu)$, through the following relationship:

$$N(\varepsilon, \mu) = \int_{-\infty}^{\varepsilon} d\varepsilon n(\varepsilon, \mu). \quad (2)$$

The notation highlights the implicit μ dependence of the DOS that arises from the effective Kohn–Sham potential. In a frozen ion treatment, of course, the nuclear interaction term is just a constant that is included here for future convenience.

The basic idea underlying the MST is partitioning the system in “small” scattering volumes, v_i , $\sum_i v_i = V$, which in most implementations are “centered” at the nuclei positions. Although at this stage the partitioning is quite arbitrary, as we shall see in the following, there is a natural choice for it. By using Lloyd’s formula,^{33,34} the integrated DOS, $N(\varepsilon; \mu)$, can be expressed as the excess with respect to the corresponding free electron quantity, $N^0(\varepsilon)$,

$$N(\varepsilon; \mu) = N^0(\varepsilon) - \frac{1}{\pi} \text{Im} \log \det \underline{M}(\varepsilon) = N^0(\varepsilon) + \frac{1}{\pi} \text{Im} \sum_i \text{Tr}[\log \underline{T}(\varepsilon)]_{ii}, \quad (3)$$

where the trace is taken only over the angular momentum components. In Eq. (3), the multiple scattering matrix \underline{M} or the scattering-path matrix³⁵ $\underline{T} = \underline{M}^{-1}$ are defined in terms of the single-site scattering matrices⁷¹ $\underline{T}_i(\varepsilon)$, and the free electron propagator $\underline{G}_{ij}^0(\varepsilon)$ is given by

$$\underline{M}_{ij}(\varepsilon) = \underline{T}_i^{-1}(\varepsilon) \delta_{ij} - \underline{G}_{ij}^0(\varepsilon). \quad (4)$$

It is convenient to recall here that the single-site scattering matrices convey the information about the phase shifts at the surfaces delimiting each scattering volume. The continuity of the wave functions at the same surfaces is ensured by the construction of the scattering-path matrix \underline{T} ; this is accomplished by the numerical inversion of the multiple scattering matrix \underline{M} . Since the size of \underline{M} is proportional to the number of scatterers in the problem, its inversion is the source of $O(N^3)$ scaling in the MST version of the DFT.

Within MST, the link between the electronic density and the scattering matrices is provided by the Green function⁶

$$\begin{aligned} G_{ij,LL'}(\mathbf{r}, \mathbf{r}', \varepsilon) &= Z_{i,L}(\mathbf{r}, \varepsilon) \tau_{ij,LL'}(\varepsilon) Z_{j,L'}(\mathbf{r}', \varepsilon) \\ &\quad - [\theta(r-r') Z_{i,L}(\mathbf{r}, \varepsilon) J_{j,L'}(\mathbf{r}', \varepsilon) \\ &\quad + \theta(r'-r) J_{i,L}(\mathbf{r}, \varepsilon) Z_{j,L'}(\mathbf{r}', \varepsilon)] \delta_{LL'} \delta_{ij}, \end{aligned} \quad (5)$$

where $\mathbf{r} \in v_i$, $\mathbf{r}' \in v_j$. $Z_{i,L}(\mathbf{r}, \varepsilon)$ and $J_{i,L}(\mathbf{r}, \varepsilon)$ are, respectively, regular and irregular at $\mathbf{r}=0$ solutions⁷² of the KS Schrödinger equation for the energy ε . For real energies, both $Z_{i,L}(\mathbf{r}, \varepsilon)$ and $J_{i,L}(\mathbf{r}, \varepsilon)$ are real functions. The (site resolved) charge densities, the DOS, and the neat charges at the i th site can be obtained by integrating the Green function over the energy and/or the appropriate volumes and by taking the trace over the angular momentum indices as follows:

$$\rho_i(\mathbf{r}; \mu) = -\frac{1}{\pi} \int_{-\infty}^{\mu} d\varepsilon \sum_L \text{Im}[G_{ii,LL}(\mathbf{r}, \mathbf{r}' = \mathbf{r}; \varepsilon)], \quad (6)$$

$$n_i(\varepsilon; \mu) = -\frac{1}{\pi} \int_{v_i} d\mathbf{r} \sum_L \text{Im}[G_{ii,LL}(\mathbf{r}, \mathbf{r}' = \mathbf{r}; \varepsilon)]. \quad (7)$$

As is shown in Refs. 22, 32, and 36, the Hohenberg–Kohn density functional [Eq. (1)] can be more conveniently rewritten within the MST formalism as the sum of a kinetic and a potential energy functional as follows:

$$\Omega(T=0, V, \mu) = T - \mu N + U, \quad (8)$$

where the above two contributions are given by the following expressions:

$$T - \mu N = -\int_{-\infty}^{\mu} d\varepsilon N(\varepsilon; \mu) - \int_V d\mathbf{r} \rho(\mathbf{r}; \mu) v^{eff}(\mathbf{r}; \mu), \quad (9)$$

$$\begin{aligned} U &= \frac{e^2}{2} \int_V d\mathbf{r} \int_V d\mathbf{r}' \frac{\rho(\mathbf{r})\rho(\mathbf{r}')}{|\mathbf{r}-\mathbf{r}'|} - \sum_j \int_V d\mathbf{r} \frac{e^2 Z_j \rho(\mathbf{r})}{|\mathbf{r}-\mathbf{R}_j|} \\ &\quad + \int_V d\mathbf{r} \rho(\mathbf{r}) e^{XC}(\mathbf{r}, [\rho]) + \frac{e^2}{2} \sum_{ij(i \neq j)} \frac{Z_i Z_j}{R_{ij}}. \end{aligned} \quad (10)$$

The effective potential in Eq. (9), $v^{eff}(\mathbf{r})$, is specified by the Kohn–Sham equation

$$v^{eff}(\mathbf{r}) = \int_V d\mathbf{r}' \frac{e^2 \rho(\mathbf{r}')}{|\mathbf{r}-\mathbf{r}'|} - \sum_j \frac{e^2 Z_j}{|\mathbf{r}-\mathbf{R}_j|} + v^{XC}(\mathbf{r}, [\rho]). \quad (11)$$

It consists of the Coulombian potential due to the electronic and ionic charges and of the exchange-correlation potential $v^{XC}(\mathbf{r}, [\rho]) = \delta E^{XC}[\rho] / \delta \rho(\mathbf{r})$, where $E^{XC}[\rho]$ is the third term on the right-hand side of Eq. (10). In the LDA, v^{XC} is assumed to depend locally on the electronic density, i.e., $v^{XC}(\mathbf{r}, [\rho]) = v^{XC}[\rho(\mathbf{r})]$ and $e^{XC}(\mathbf{r}, [\rho]) = e^{XC}[\rho(\mathbf{r})]$.

We wish to highlight a useful consequence of the above partitioning of the system volume. The density functional defined by Eq. (8), which is, of course, variational with respect to the global charge density $\rho(\mathbf{r})$, turns out to be variational also with respect to the charge densities in each scattering volume v_i as follows:

$$\frac{\delta \Omega}{\delta \rho_i(\mathbf{r})} = 0. \quad (12)$$

Furthermore, it is possible to show³² that

$$\frac{\delta U}{\delta \rho_i(\mathbf{r})} = v_i^{eff}(\mathbf{r}; \mu) \quad (13)$$

and that

$$\frac{\delta(T - \mu N)}{\delta \rho_i(\mathbf{r})} = -v_i^{eff}(\mathbf{r}; \mu). \quad (14)$$

It is interesting to observe that the expression for the site resolved DOS [Eq. (7)] allows us to recast the integrated DOS and the electronic grand potential as sums of site resolved contributions. These contributions, however, involve the site-diagonal part of the system Green function or scattering matrix, \underline{G}_{ii} or \underline{T}_{ii} , and then are nontrivially coupled together through the boundary conditions. If this coupling was neglected, as it is done, for instance, in the case of the Harris–Foulkes density functional,¹² $O(N)$ scaling could be obtained. Fortunately, similar numerical performances can be achieved with less dramatic approximations. A sensible alternative is to impose *random* boundary conditions at the fragment surfaces.¹¹ In this paper, we shall follow a different approach and use *averaged* boundary conditions. As we shall see in the following section, this allows us to have a tractable form for the coupling in the kinetic part of the density functional and permit to obtain $O(N)$ algorithms. Although it was proposed with a different aim, one of the oldest method applying such mean boundary conditions is the CPA, a generalized version of which shall be offered in the next section. Before, however, we need to discuss a different source of coupling that is present in the potential energy part of the

functional, namely, the electrostatic interactions between fragments. In the past, this subject has received little consideration and it has been ruled out by invoking the screening properties of metals. However, nowadays, there is a general consensus that careful estimates of these interactions are necessary in order to obtain accurate total energies for metallic alloys.

B. Multipole expansions for the effective potentials and the potential energy

We have shown in Sec. II A that the DF-MST theory is variational with respect to the local charge densities $\rho_i(\mathbf{r})$ of each fragment or scattering volume. In this subsection, we shall see how the multipole expansion used by most numerical implementations of the theory has the conceptual advantage of giving expressions for the effective Kohn–Sham potentials and the potential energy in which different scattering volumes are coupled together only through simple functions of the multipole moments.

The relevant formulas can be obtained by splitting the volume integrals in Eqs. (10) and (11) in sums of integrals extending over the scattering volumes v_i and by expanding the denominators in spherical harmonics. Although they require some labor, the derivations are very straightforward and need not be reported here. The resulting expressions for the potential energy and the effective potentials are listed below,

$$U = \sum_i \left\{ u_i[\rho_i(\mathbf{r})] + \frac{e^2}{2} \sum_L q_{i,L} V_{i,L}^{Mad} \right\} \quad (15)$$

and

$$v_i^{eff}(\mathbf{r}) = e^2 \int_{v_i} d\mathbf{r}' \frac{\rho_i(\mathbf{r}')}{|\mathbf{r} - \mathbf{r}'|} - \frac{e^2 Z_i}{r} + v^{XC}[\rho_i(\mathbf{r})] + e^2 V_i^{Mad}(\mathbf{r}). \quad (16)$$

In Eqs. (15) and (16), we have introduced the local multipole moments,

$$q_{i,L} = \int_{v_i} d\mathbf{r} \rho_L(\mathbf{r}) \rho_i(\mathbf{r}) - Z_i \delta_{L,(0,0)}, \quad (17)$$

and the Madelung potentials,

$$V_i^{Mad}(\mathbf{r}) = \sum_L V_{i,L}^{Mad} p_L(\mathbf{r}), \quad (18)$$

where

$$V_{i,L}^{Mad} = \sum_{j \neq i} \sum_{L'} M_{ij,LL'} q_{j,L'}. \quad (19)$$

The coefficients $M_{ij,LL'} = M_{LL'}(\mathbf{R}_{ji})$ are given by

$$M_{LL'}(\mathbf{R}) = 4\pi \sum_{L''(\ell''=\ell+\ell')} C_{LL'}^{L''} \frac{(2\ell''+1)!!}{(2\ell''+1)} \frac{Y_{L''}(\hat{\mathbf{R}})}{R^{\ell''+1}}, \quad (20)$$

where $C_{LL'}^{L''}$ are the Gaunt numbers,³⁷ and the functions $p_L(\mathbf{r})$ in Eq. (16) are defined as

$$p_L(\mathbf{r}) = \frac{\sqrt{4\pi}}{(2\ell+1)!!} r^\ell Y_L^*(\mathbf{r}). \quad (21)$$

The only values that are relevant for spherical approximations are $p_{00}(\mathbf{r})=1$ and $M_{00,00}(R)=1/R$.

In Eq. (15), the contribution from the i th lattice site to the potential energy is denoted as $u_i([\rho_i(\mathbf{r})])$ and given by

$$u_i([\rho_i(\mathbf{r})]) = \frac{e^2}{2} \int_{v_i} d\mathbf{r} \int_{v_i} d\mathbf{r}' \frac{\rho_i(\mathbf{r}) \rho_i(\mathbf{r}')}{|\mathbf{r} - \mathbf{r}'|} - \int_{v_i} d\mathbf{r} \frac{e^2 Z_i \rho_i(\mathbf{r})}{r} + \int_{v_i} d\mathbf{r} \rho_i(\mathbf{r}) e^{XC}[\rho_i(\mathbf{r})]. \quad (22)$$

Within the LDA, u_i depends on the electronic density at the i th fragment only, while for nonlocal approximations to the DFT, there could be some dependence on the density at sites $j \neq i$.

Much published work has been done within spherical approximations (SAs), namely, the muffin-tin (MT) or the atomic sphere approximation (ASA). In that case, only the first terms, $\ell=0$, of the multipole expansions are included. Thus, Eqs. (15) and (16) must be replaced by the following expressions:

$$U = \sum_i \left(u_i\{\rho_i(\mathbf{r})\} + \frac{e^2}{2} q_i V_i^{Mad} \right) \quad (23)$$

and

$$v_i^{eff}(\mathbf{r}) = \int_{v_i} d\mathbf{r}' \frac{e^2 \rho_i(\mathbf{r}')}{|\mathbf{r} - \mathbf{r}'|} - \frac{e^2 Z_i}{r} + v^{XC}[\rho_i(\mathbf{r})] + e^2 V_i^{Mad}. \quad (24)$$

Thus, for SAs, the only relevant multipole moments are the local charge excesses,

$$q_i \equiv q_{i,00} = \int_{v_i} d\mathbf{r} \rho_i(\mathbf{r}) - Z_i, \quad (25)$$

and the Madelung potentials are constant within each scattering volume to the values

$$V_i^{Mad} \equiv V_{i,00}^{Mad} = \sum_{j \neq i} \frac{q_j}{R_{ij}}. \quad (26)$$

Remarkably, in Eqs. (15) and (16) or in their SA counterparts [Eqs. (23) and (24)], the charge densities at different sites, $\rho_i(\mathbf{r})$, are coupled only with the Madelung potentials at the same sites, $V_i^{Mad}(\mathbf{r})$. Of course, the last quantities contain information about the charge densities at all crystal sites.

We wish to highlight that the multipole expansion does not converge for arbitrary partitions of the system. Actually, convergence requires that for any pair of scattering centers, \mathbf{R}_i and \mathbf{R}_j , and for any point \mathbf{r} belonging to the scattering volume v_i , the triangular inequality illustrated in Fig. 1 must be satisfied. It is easy to realize that partitioning of the system in Voronoi polyhedra accordingly with the Wigner–Seitz construction guarantees the above condition to be fulfilled everywhere except but for the zero measure set of points constituted by the surfaces of the polyhedra, thus ensuring

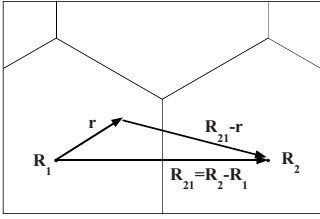


FIG. 1. Triangular inequalities that must be satisfied in order to have a convergent multipole expansion: $r < |\mathbf{r} - (\mathbf{R}_2 - \mathbf{R}_1)|$, $r < |\mathbf{R}_2 - \mathbf{R}_1|$. The partition of the system volume in Voronoi polyhedra marked by the lines guarantees that the inequalities hold.

the convergence of the theory. The Wigner–Seitz construction therefore constitutes a natural choice for the partitioning.

III. GENERALIZED COHERENT-POTENTIAL APPROXIMATIONS AND CHARGE-EXCESS FUNCTIONAL THEORY

A. Generalized coherent-potential approximations for the scattering matrices

In this section, we shall discuss a whole class of approximations for systems with atoms lying on a regular lattice, where, however, substitutional disorder is allowed for. Metallic alloys, both ordered intermetallic compounds and random alloys, constitute the most relevant example of such systems. Other examples are crystals with empty, or “vacancy,” sites. Although, in general, these systems do not have translational invariance, nevertheless, the underlying “geometrical lattice” does. Forty years ago, this consideration led Soven to formulate the CPA.²⁰ Since then, the CPA had an appreciable fortune. Its crucial virtue was that by introducing a “mean field” fashion effective crystal, it allows us to use many techniques designed for ordered systems that were already well developed at the time at which the theory was proposed.

For many years, the DFT implementations of the CPA^{22,38} have been based on the assumption (in the following referred to as the isomorphous approximation or I) that sites occupied by atoms of the same chemical species are characterized by the same effective Kohn–Sham potentials. Although the DFT-I-CPA has been proved able to carefully determine the electronic structure and the spectral properties of many alloy systems,^{25,39,40} nevertheless, it leads to an incorrect description of the electrostatics and of the total energies in metallic alloys.⁴¹ Due to its mean field nature, in fact, the isomorphous approximation neglects the fluctuations of the charge transfers and the energetic electrostatic contributions associated with them. This failure has stimulated many authors that envisaged CPA generalizations aimed to include the effects of different chemical environments.^{42–46}

In this paper, we define a *class of approximations* for DFT-based electronic theories in which most of the above CPA generalizations can be included. We shall refer to the approximations belonging to such a class as GCPA. A theory belonging to the GCPA class shall be identified by (a) a theory specific *external model*, i.e., a rule for determining the effective Kohn–Sham “site” potentials and the statistical

weights w_i to be assigned to each site, and (b) an approximate form for the kinetic part of the density functional specified by Eqs. (27)–(30) below. The last feature is common to all the theories belonging to the GCPA class.

Before discussing the ansatz for the kinetic functional, we wish to illustrate what a GCPA “external model” can be on the basis of a few examples. The first example of a GCPA theory is, of course, the DFT implementation of the I-CPA in Refs. 22 and 32. Its external model is the isomorphous assumption (identical effective potentials for atoms of the same atomic species and weights proportional to the respective atomic concentrations). Another example is the polymorphous CPA (PCPA) of Ujfalussy *et al.*^{43,47,48} The external model is constructed by using an auxiliary supercell containing N atoms, usually hundreds or thousands, each to be weighted with the same weight. The effective site potentials are reconstructed on the same supercell via Eq. (11); thus, atoms of the same chemical species are allowed to have different potentials depending on their environments. This specific choice for the external model appears to be the reason why the PCPA theory substantially improves the alloy electrostatics while maintaining all the advantages of the standard I-CPA about the spectral properties.⁴⁹ Other existing CPA-based approaches, e.g., the nonlocal CPA^{50,51} or the SIM-CPA,^{44,45} can also be considered as particular cases of GCPAs.

We shall now introduce the kinetic ansatz that is common to all GCPA theories. For this purpose, we prefer not to start from the definition of the functional. Rather, we shall follow a path closer to physical intuition and to the spirit of Soven’s original CPA formulation.²⁰ At the similarity of I-CPA calculations, the GCPA defines an effective periodic crystal whose sites are occupied by effective “coherent” scatterers characterized by the single-site scattering matrix $\underline{t}^c(\varepsilon)$; the corresponding Green function shall be $G^c(\underline{t}^c)$. Then, if we consider the Green function of a single substitutional impurity with a single-site scattering matrix \underline{t}_i embedded in the above effective crystal, $G_{ii}(\underline{t}_i, \underline{t}^c)$, the GCPA consists in requiring that

$$\sum_i \frac{w_i}{N} G_{ii}(\underline{t}_i, \underline{t}^c) = G^c(\underline{t}^c). \quad (27)$$

In other words, the weighted average of the impurity Green functions must be equal to the coherent Green function $G^c(\underline{t}^c)$. In Eq. (27), the energy dependences have been dropped for the sake of simplicity and N stands for the number of different scatterers in the model.

Equation (27) is illustrated in Fig. 2. In terms of the coherent scattering-path matrix of the effective lattice $\underline{\tau}^c$ and of the CPA projectors D_i , it can be rearranged as follows:

$$\sum_i \frac{w_i}{N} D_i = \underline{1}, \quad (28)$$

$$D_i = \{ \underline{1} + [(\underline{t}_i)^{-1} - (\underline{t}^c)^{-1}] \underline{\tau}^c \}^{-1}. \quad (29)$$

A GCPA theory is then an approximation for the $\underline{\tau}$ matrix, whose diagonal elements are given by

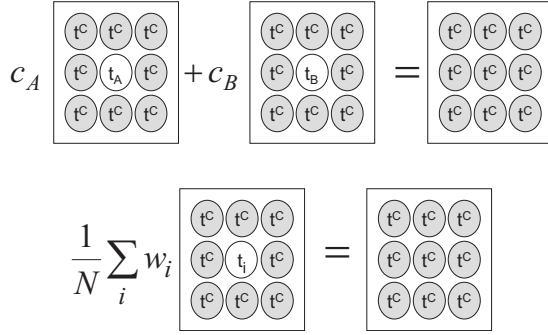


FIG. 2. A pictorial illustration of the isomorphous CPA for a binary, $A_{c_A}B_{c_B}$, alloy (top) and of the GCPA (bottom). The rectangular frames have the meaning “the Green function of what is inside.”

$$\tau_{ii} = \underline{D}_i \underline{\tau}^c, \quad (30)$$

while the diagonal matrix elements of the Green function are given by Eq. (5) with $i=j$.

Within the approximation defined by Eqs. (27)–(30) above, the MST reviewed in the previous section allows us to calculate the charge densities and the integrated DOS, $N(\varepsilon, \mu)$, and, through Eq. (9), the kinetic part of the Hohenberg–Kohn functional. Here, we need not to trace all the intermediate steps that can be reproduced following the scheme of Ref. 32. The GCPA approximate version of the Lloyd formula [Eq. (4)] is given by

$$\begin{aligned} \frac{N(\varepsilon; \mu)}{N} &= \frac{N^0(\varepsilon)}{N} + \frac{1}{\pi} \text{Im} \sum_i w_i \text{Tr} \log \underline{\tau}^c(\varepsilon) \\ &+ \frac{1}{\pi} \text{Im} \sum_i w_i \text{Tr} \log \underline{D}_i(\varepsilon). \end{aligned} \quad (31)$$

It has the very remarkable property that the integrated DOS $N(\varepsilon; \mu)$ and, hence, the kinetic functional are variational³² with respect to both $\underline{\tau}^c$ and $\underline{\tau}$.

In Sec. II A, we have mentioned that in the exact MST, the contributions to the integrated DOS associated with each lattice site and proportional to $(\log \underline{\tau})_{ii}$ are coupled together because each element of the $\underline{\tau}$ matrix depends on the scattering properties of all the lattice sites. Within the GCPA, the only source of coupling is $\underline{\tau}^c$. Each local contribution depends on $\underline{\tau}^c$ and on the local potential. However, within the GCPA, the Lloyd formula does not depend on $\underline{\tau}^c$ nor on the local potentials. As a consequence, the integrated DOS results in a sum of local contributions, coupled together only through $\underline{\tau}^c$,

$$N(\varepsilon; \mu) = \sum_i w_i N_i(\varepsilon; \mu). \quad (32)$$

We shall call this very controlled and tractable kind of coupling as the *marginal coupling*.

In view of further developments, it is convenient to isolate in Eq. (32) two distinct terms. The first arises from the first two addends in Eq. (31); it is identical for all sites and related to the effective background defined by the GCPA medium. The second depends on the local CPA projectors and,

through them, on the local potentials. In formula,

$$N_i(\varepsilon; \mu) = N_i^{\text{back}}(\varepsilon; \mu) + \frac{1}{\pi} \text{Im} \text{Tr} \log \underline{D}_i(\varepsilon). \quad (33)$$

Implementing the GCPA within the DFT gives for the kinetic functional of Eq. (9) the following marginally coupled form:

$$T - \mu N = T^{\text{back}}(\mu) + \sum_i w_i T_i([\rho_i], \mu), \quad (34)$$

where

$$T^{\text{back}}(\mu) = - \int_{-\infty}^{\mu} d\varepsilon N^{\text{back}}(\varepsilon; \mu) \quad (35)$$

and

$$\begin{aligned} T_i([\rho_i], \mu) &= \frac{1}{\pi} \text{Im} \text{Tr} \int_{-\infty}^{\mu} d\varepsilon \log \underline{D}_i(\varepsilon) \\ &- \int_{v_i} d\mathbf{r} \rho_i(\mathbf{r}; \mu) v_i^{\text{eff}}(\mathbf{r}; \mu). \end{aligned} \quad (36)$$

As mentioned in Sec. II, in MST-based DFT calculations, the only source for $O(N^3)$ scaling is the inversion of the multiple scattering matrix [Eq. (4)] required to obtain the scattering-path matrix $\underline{\tau}$. This step is bypassed in a GCPA theory by approximating the relevant matrix elements τ_{ii} via Eq. (28) in terms of the local scattering properties and the coherent scattering matrix $\underline{\tau}^c$, the last of which is, in turn, obtained by an averaging process. For this reason, GCPA theories are $O(N)$, allowing for very substantial savings of computing time. Of course, the price for these savings is paid by the approximation implied by Eq. (30). A diagrammatic analysis of these errors can be found in Ref. 6.

It is necessary to make a couple of remarks about the physical meaning of the GCPA in the present context and to highlight the differences with respect to the traditional way in which CPA-based theories have been introduced in the past. In the first place, the GCPA has been introduced here as an approximation for the Hohenberg–Kohn density functional. As an approximation, it may well be used to describe an ordered alloy. Its range of applicability is by no means confined to the realm of random alloys. In the second place, the introduction of the weights w_i that are assigned to each scatterer makes GCPA theories suitable for dealing with sophisticated pictures of the order (or the disorder) in metallic alloys. This, of course, requires what we have called an “external model.” In a foregoing paper, we shall discuss a (to some extent) self-consistent way to define an external model that is able to provide a picture of ordering phenomena in metallic alloys as a function of the temperature.

B. Density functional theory–multiple scattering theory–generalized coherent potential approximation functional: The marginal coupling property

In the present subsection, we shall analyze certain formal properties of the GCPA approximations introduced in the

previous subsection. All the above discussions can be summarized in the following GCPA density functional:

$$\Omega^{GCPA} = T^{back}(\mu) + \sum_i w_i \left[\omega_i^{GCPA}([\rho_i], \mu) + \frac{e^2}{2} \sum_L q_{i,L} V_{i,L}^{Mad} \right], \quad (37)$$

which results from the application of the GCPA to the exact DFT-MST density functional.

In Eq. (37), the $q_{i,L}$ are defined by Eq. (17), and the *local part* of the GCPA functional by

$$\omega_i^{GCPA}([\rho_i], \mu) = T_i([\rho_i], \mu) + u_i([\rho_i], \mu), \quad (38)$$

where the terms $T_i([\rho_i], \mu)$ and $u_i([\rho_i], \mu)$ are given by Eqs. (36) and (22) above. We note that the local GCPA functional ω_i^{GCPA} also depends on the atomic number of the atom at \mathbf{R}_i , Z_i , and on the volume and the shape of the i th Voronoi polyhedron through the local potential energy term, u_i . In the following, we shall make the simplifying assumption of having identical Voronoi polyhedra for all the sites considered that is equivalent to neglect local lattice deformations.

In Eq. (37) the coupling potentials, $V_{i,L}^{Mad}$, are provided by the specific external model. In the following, we shall assume

$$V_{i,L}^{Mad} = \sum_{j \neq i} \sum_{L'} \lambda_L \lambda_{L'} w_j M_{ij,LL'} q_{j,L'}. \quad (39)$$

Appropriate choices of the coefficients λ_L and of the weights w_j give then the I-CPA or the PCPA. Furthermore, Eq. (39) can also be used for spherical or for full-potential charge reconstructions.

As mentioned in Sec. II A [Eq. (12)], the density functional is variational not only with respect to the global charge density $\rho(\mathbf{r})$ and the chemical potential μ but also with respect to the charge densities in each scattering volume, $\rho_i(\mathbf{r})$. Moreover, as discussed in Sec. III A and in Ref. 32, the GCPA density functional is variational with respect to the effective medium scattering matrix \mathcal{T}^c . Furthermore, in a GCPA theory, the background kinetic term $T^{back}(\mu)$ in Eq. (37) depends on the electronic density only through \mathcal{T}^c and μ . Thus, the functional derivation of Eq. (37) with respect to the local densities $\rho_i(\mathbf{r})$ gives the following set of coupled equations:

$$\frac{\delta \omega_i^{GCPA}}{\delta \rho_i(\mathbf{r})} + V_i^{Mad}(\mathbf{r}) = 0, \quad (40)$$

where we have used Eqs. (17)–(19) and (21).

Within a GCPA theory, solving the set of the Euler–Lagrange equations [Eq. (40)], one for each scattering center together with the equations that determine the chemical potential and the coherent scattering matrix \mathcal{T}^c , is completely equivalent to the minimization of the density functional. As it is apparent, these Euler–Lagrange equations are coupled to each other *only* through the Madelung potentials, \mathcal{T}^c and μ . Moreover, the functionals $\omega_i^{GCPA}[\rho_i(\mathbf{r})]$ are identical for sites occupied by the same chemical species.

In order to understand the consequences of the above result, let us consider, for instance, an alloy sample constituted

by a large supercell. One may wish to calculate, *in the given sample*, the properties of different atoms, in the first place the charge densities $\rho_i(\mathbf{r})$. Inside the sample, \mathcal{T}^c , μ , and the cell geometry are fixed; thus, the set of the $\rho_i(\mathbf{r})$ is completely determined by the values of the Madelung potentials $V_i^{Mad}(\mathbf{r})$ and by the atomic number Z_i of the ion at the position \mathbf{R}_i . More generally, inside the given sample, any site-diagonal property Π_i shall be completely determined by Z_i and by the set of Madelung potentials. We can establish this result as follows:

$$\Pi_i = \Pi[Z_i, V_i^{Mad}(\mathbf{r})]. \quad (41)$$

Examples of such site-diagonal properties are the local contributions to the grand potential, the multipole moments, and the local DOS. The functional forms, one for each alloying species, given by Eq. (41) sometimes can be easily numerically fitted and then constitute a useful tool for the evaluation of the site quantities in the given sample. They are the source of the simple laws as, e.g., the qV laws, empirically found from extended metallic system calculations. This notwithstanding, GCPA theories are able to predict complex trends for certain site-diagonal properties as, e.g., the site resolved DOSs.^{49,52}

Since Eq. (41) allows us to evaluate, among other properties, also the charge density of each fragment and, hence, the full charge density $\rho(\mathbf{r})$, then, in virtue of the Hohenberg and Kohn theorem, it follows that any ground state observable in the sample given is a *functional* of the set of the Madelung potentials at all the crystal sites, $V_i^{Mad}(\mathbf{r})$, and of the set of the atomic numbers *only*. Since the last is, again, specified by the sample, it follows the theorem *any ground state observable in the sample given is a functional of the Madelung potentials only* or, equivalently, *a function of the set of coefficients*, $\{V^{Mad}\}$, that completely determine the Madelung potentials.⁷³

Since, in virtue of Eq. (39), the coefficients in the set $\{V^{Mad}\}$ are linear functions of the set of the multipole moments, $\{q\}$, then the above theorem implies the corollary that any ground state property of the sample is a function of the same moments. Within the GCPA and for the specific sample given, it is then possible to reformulate the DFT in terms of the charge multipole moments. By neglecting a constant term with the physical meaning of the grand potential contribution due to the mean GCPA “atom,” Eq. (37) can be written as

$$\begin{aligned} \tilde{\Omega}^{GCPA}(\{q\}, \mu) &= \sum_i w_i \tilde{\omega}_i^{GCPA}(\{q_i\}, Z_i) \\ &+ \frac{e^2}{2} \sum_{i,j,L,L'} w_i w_j \lambda_L \lambda_{L'} M_{ij,LL'} q_{i,L} q_{j,L'} \\ &- \mu \sum_i w_i q_{i,00}. \end{aligned} \quad (42)$$

In deriving Eq. (42), we have used Eq. (39) and the fact that since ω_i^{GCPA} is completely determined by the local density $\rho_i(\mathbf{r})$, it cannot depend on the multipole moments at other sites. Moreover, we have isolated the contribution proportional to the chemical potential μ . Having introduced an explicit dependence on μ , the last term in Eq. (42) can be

thought as a way of enforcing the global electroneutrality. This is unnecessary if we consider a specified sample in which, of course, μ has a precise fixed value. However, since the term proportional to μ has precisely the form it must have, its introduction is equivalent to extend the validity of Eq. (42) to *all samples specified by the same mean atomic concentrations and by the same value for τ^c* .

To summarize, we have established the following exact results. Within the GCPA class of approximations, the Hohenberg and Kohn density functional can be recast in the form of Eq. (42). It consists of (a) local terms, $\tilde{\omega}_i^{GCPA}$ for the i th scattering site, consisting in functions of the charge multipole moments that are identical for sites with the same chemical occupation; (b) a bilinear form coupling the charge multipole moments at different sites, with coupling coefficients $M_{ij,LL'}$ defined by the crystal geometry; (c) and a term proportional to the chemical potential that ensures the global electroneutrality. The functional defined by Eq. (42) is identical for all the alloy samples characterized by the same mean atomic concentrations and the same value for the coherent scattering-path matrix τ^c . Evidently, it constitutes a coarse-grained version of the DFT because the mathematical definition of the multipole moments [Eq. (17)] does not completely determine the charge density. The last is determined by the multipole moments only within the GCPA theory. This reduction of the relevant information has been obtained at the price (a) of the GCPA approximation and (b) of having restricted the consideration to a specific sample. Nevertheless, no restriction has been made about the size of the sample that, therefore, can be chosen in such a way to guarantee an appropriate description for a fixed concentration ensemble, as we shall discuss at the end of the present section.

Having recast the GCPA functional as a sum of *functions* of the charge multipole moments has obvious mathematical advantages. However, we have not yet completely determined the functional form of the local energetic contributions $\tilde{\omega}_i^{GCPA}(\{q_i\}, Z_i)$. In order to do this, we need to make the hypothesis that in the sample considered, the distribution of the Madelung potential coefficients $\{V^{Mad}\}$ is continuous in the range of the values that the same potentials assume in the sample. This is consistent with the observations in Refs. 23,24,26. Let us consider two scattering sites, say, i and j , occupied by the same chemical species α , at which the Madelung coefficients take very close numerical values, $V_{i,L}^{Mad} = V_L^{Mad}$ and $V_j^{Mad}(\mathbf{r}) = V^{Mad}(\mathbf{r}) + \Delta V^{Mad}(\mathbf{r})$. The local energetic contributions, the charge densities, and the local multipole moments shall be $\tilde{\omega}_i^{GCPA} = \tilde{\omega}_\alpha^{GCPA}$, $\rho_i(\mathbf{r}) = \rho(\mathbf{r})$, and $q_{i,L} = q_L$ for the i th site and $\tilde{\omega}_j^{GCPA} = \tilde{\omega}_\alpha^{GCPA} + \Delta \tilde{\omega}_\alpha^{GCPA}$, $\rho_j(\mathbf{r}) = \rho(\mathbf{r}) + \Delta \rho(\mathbf{r})$, and $q_{j,L} = q_L + \Delta q_L$ for the j th site. To the first order in $\Delta \rho(\mathbf{r})$, we have

$$\begin{aligned} \Delta \tilde{\omega}_\alpha^{GCPA} &= \int_{v_i=v_j} d\mathbf{r} \left[\frac{\delta \tilde{\omega}_\alpha^{GCPA}}{\delta \rho(\mathbf{r})} \right]_{\rho_i(\mathbf{r})=\rho(\mathbf{r})} \Delta \rho(\mathbf{r}) \\ &= - \int_{v_i=v_j} d\mathbf{r} V^{Mad}(\mathbf{r}) \Delta \rho(\mathbf{r}), \end{aligned}$$

where Eq. (40) has been used. The substitutions of the expansion for the Madelung potential [Eq. (18)] and of the

expressions for the charge multipole moments [Eq. (17)] then give

$$\Delta \tilde{\omega}_\alpha^{GCPA} = - \sum_L V_L^{Mad} \Delta q_L. \quad (43)$$

Once integrated over q_L , Eq. (43) gives

$$\tilde{\omega}_\alpha^{GCPA}(\{q\}) = \tilde{\omega}_\alpha^{GCPA}(\{q^0\}) - \sum_L \int_{\{q^0\}}^{\{q\}} V_{L,\alpha}^{Mad}(\{q'\}) dq'_L. \quad (44)$$

Equation (44) can be easily numerically evaluated from the qV data, $V_{L,\alpha}^{Mad} = V_{L,\alpha}^{Mad}(\{q\})$, obtained as an output from GCPA calculations. Unless constant with the meaning of the local energy contribution at $\{q\} = \{q^0\}$, it determines the local energies for each chemical species α . Equations (43) and (44) have been obtained under very broad conditions: the differentiability of the kinetic functional^{53,54} and the monotonicity of the qV laws. The first is the usual requirement for the convergence of the Kohn–Sham scheme of the DFT, while the second condition is certainly verified by all GCPA calculations reported in the literature, including those executed at extremely high values for the Madelung potential (see Fig. 7 in the next subsection and the related discussion).

In the remainder of the present section, we shall make a few general comments about the validity of the framework defined by the GCPA theory in comparison with the exact density functional.

(i) The fact that the effective potential and the potential energy functional can be decomposed in site contributions coupled together only through the Madelung potentials is an exact consequence of the LDA and it has nothing to do with the GCPA. This kind of coupling is *marginal* in the sense that, although not necessarily small, it has the simple and tractable functional form, which arises from the bilinear terms involving the multipole moments in Eq. (42). Although this is beyond the purpose of the present paper, we notice that most nonlocal density functionals offered in the literature^{3,5} are actually local with respect to the density gradients; thus, most nonlocal schemes will remain *marginally* coupled in the above sense.

(ii) Splitting the kinetic functional into local contributions marginally coupled through the coherent scattering matrix τ^c is a simplification due to the GCPA. In fact, it has been obtained by assuming averaged boundary conditions at the surfaces of the Voronoi polyhedra through Eq. (27). An estimate of the so induced errors can be obtained by the comparison of PCPA vs locally self-consistent Green function (LSGF) calculations¹⁷ executed on the same supercell. As it is sketched in Fig. 3, both calculations evaluate the kinetic contribution from the i th site to the functional by solving the problem of a single impurity, in the case of the PCPA, or of an impurity cluster, the LIZ, for the LSGF. In both cases, the scattering matrices outside the LIZ are set to the coherent scattering matrix τ^c . PCPA calculations can then be viewed as LSGF calculations with only one atom in the LIZ. This argument also suggest that with respect to GCPA calculations, exact DFT results include, for each site, corrections depending on its chemical environment.

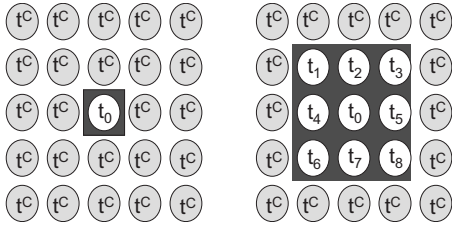


FIG. 3. The LIZs used in PCPA (left frame) and LSGF (right frame) calculations are marked by the dark areas. For each scattering site, the kinetic functional is evaluated by using the appropriate single-site scattering matrices t_i inside the LIZ and the effective CPA scattering matrix t^c outside.

(iii) We have already seen that the coarse-grained version of the GCPA functional [Eq. (42)] holds for all the alloy configurations characterized by a specified value for \mathcal{Z}^c in a fixed concentration ensemble. This could appear as a serious limitation since it looks unlikely that, e.g., \mathcal{Z}^c could have the same functional energy dependence for two different systems. In general, in a GCPA theory, \mathcal{Z}^c is a ground state property determined not only by the mean concentrations but also by the distributions of the Madelung potentials for each alloying species. As opposite to the isomorphous model where these distributions are trivial, more sophisticated external models as, e.g., the PCPA, give complicated charge and Madelung potential distributions. How could then the GCPA functional be useful in such cases? As argued by Faulkner *et al.*,⁵⁵ the PCPA theory applied to ideal random alloys gives well-defined values for all physical properties. This is because in perfect random alloys, the distribution of the chemical environments is easily obtained by statistical considerations and it is given by the appropriate multinomial distributions. Therefore, the PCPA random alloy constitutes a privileged reference system whose physical properties, including \mathcal{Z}^c , can be approximated up to an arbitrary accuracy by letting the number of atoms in the PCPA supercell, N , approach infinity [see Fig. 4(a)]. We believe that the same \mathcal{Z}^c obtained for a random alloy at a given concentration can be used for building a physically clean, though approximate,

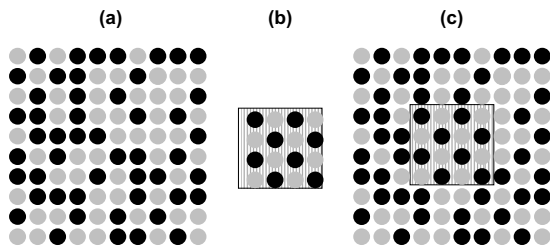


FIG. 4. The PCPA supercells shown in frames (a) and (b) contains, respectively, $N \rightarrow \infty$ atoms in a random alloy configuration and n atoms in an ordered configuration, both at the same mean atomic concentrations. N is large enough to guarantee an appropriate description of a random alloy within a GCPA theory. Similarly, n has been chosen to permit the description of an ordered alloy up to some length scale l . The supercell in the frame (c) is identical to that in (a) except but for the dashed region, which contains n atoms in the same ordered configuration as in (b). The cell (c) is therefore able to describe an ordering fluctuation up to the scale set by l .

theory also for ordered alloys at the same concentration. In the next section, we shall provide numerical evidences for that; here, we present a more formal argument. Imagine that an ordered array containing n atoms [Fig. 4(b)] is able to account for the properties of same ordered alloy configuration, up to a length scale l , that can be made large at will in the $n \rightarrow \infty$ limit. In Fig. 4(c), we draw a supercell, a part of which is constituted by the supercell of Fig. 4(b), while the remaining $N-n$ sites are occupied as in the random alloy supercell of Fig. 4(a). We can think that the supercell in Fig. 4(c) represents a fluctuation of an ordered phase in a random alloy matrix and that it describes the physical properties of such fluctuation up to the same length scale l as in Fig. 4(b). We are implicitly using the common idea of “locality” in physics or, in a more specific context, of “nearsightedness” of the DFT.⁵⁶ However, as Eq. (28) implies, the difference between the coherent scattering-path matrices corresponding to Figs. 4(a) and 4(c), $\mathcal{Z}_a^c - \mathcal{Z}_c^c$, is proportional to the ratio n/N and then it can be made small at will in the $N \rightarrow \infty$ limit, for any value of n . We conclude that the coherent scattering-path matrices of a random alloy, \mathcal{Z}_a^c , is able to account for the physical properties of ordered configuration considered. The limitation $n/N \ll 1$ that comes from the above argument does not impose any upper bound on the maximum length scale at which chemical fluctuations can be studied and it is of no practical importance provided that N is large enough to ensure a good approximation \mathcal{Z}_a^c . As reported in the literature,^{47,49} it seems that N of about 100 is already enough.

(iv) Although we have suggested that the coherent scattering matrix from random alloy GCPA calculations can be used for ordered alloys too, we are aware of the limitations of such a physical picture. For instance, a GCPA theory always implies finite quasiparticle lifetimes⁵⁷ and, hence, a smearing of the peaks of the Bloch spectral function.

C. Generalized version of the charge-excess functional theory

As a matter of fact, the analysis of DFT supercell calculations for metallic alloys suggests the existence of simple relationships between the charge excesses at the lattice sites, $q_{i,00}$, and the Madelung potentials at the same sites, $V_{i,00}^{Mad}$. Namely, simple linear laws, one for each alloying species, have been found to hold, say,

$$a_i q_{i,00} + V_{i,00}^{Mad} = k_i, \quad (45)$$

where a_i and k_i have the same numerical values for atoms of the same chemical species in the given supercell. Examples of the linear qV laws obtained from PCPA calculations for a binary and a quaternary alloy are reported in Figs. 5 and 6.

It is interesting to observe that similar linear qV laws can be derived starting from the GCPA functional [Eq. (42)] for random alloys by a second order series expansion about the zero Madelung field multipole moments, $\{q^0\}$, that can be obtained by solving the following set of equations:

$$\frac{\partial \tilde{\omega}_i^{GCPA}}{\partial q_{i,L}} = 0. \quad (46)$$

This procedure leads to a Ginzburg–Landau configurational “Hamiltonian” in which the relevant fields are constituted by

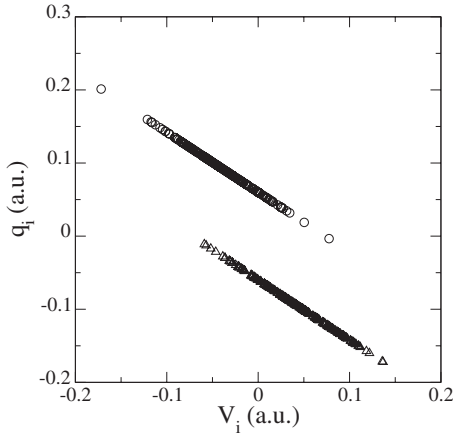


FIG. 5. qV relationships for a bcc random $\text{Cu}_{0.50}\text{Zn}_{0.50}$ alloy. The excesses of electrons, $q_i = q_{i,00}$, are plotted vs the Madelung potentials V_i^{Mad} . The results have been obtained from $\ell_{\text{max}}=0$ PCPA calculations for a supercell containing 432 atoms at lattice constant $a=5.50$ a.u. Circles represent Cu atoms and triangles represent Zn atoms. Note that positive values for q_i correspond to negative net charges and vice versa.

the values of the multipole moments of each lattice site. In formula,

$$\begin{aligned} \tilde{\Omega}^{\text{CEF}}(\{q\}, \mu) = & \frac{1}{2} \sum_{i,L,L'} w_i a_{i,LL'} (q_{i,L} - q_{i,L}^0) (q_{i,L'} - q_{i,L'}^0) \\ & + \frac{1}{2} \sum_{i,j,L,L'} w_i w_j \lambda_L \lambda_{L'} M_{ij,LL'} q_{i,L} q_{j,L'} \\ & - \mu \sum_i q_{i,00}, \end{aligned} \quad (47)$$

where we have omitted the term $\tilde{\Omega}^{\text{CEF}}(\{q^0\}, \mu=0)$ that represent the GCPA energy at zero Madelung field and chemical potential and that is constant in a fixed concentration en-

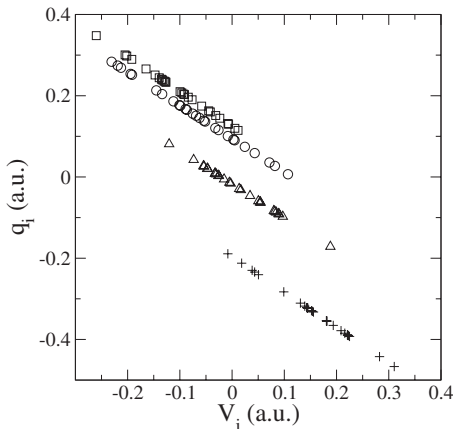


FIG. 6. qV relationships for an fcc random $\text{Al}_{0.25}\text{Cu}_{0.25}\text{Ni}_{0.25}\text{Zn}_{0.25}$ alloy. The excesses of electrons, $q_i = q_{i,00}$, are plotted vs the Madelung potentials V_i^{Mad} . The results have been obtained from $\ell_{\text{max}}=0$ PCPA calculations for a bcc supercell containing 108 atoms at lattice constant $a=6.88$ a.u. Circles, squares, triangles, and crosses stand for Cu, Ni, Zn, and Al atoms.

semble. The coefficients $a_{i,LL'}$ are given by the second derivatives of the GCPA functional

$$a_{i,LL'} = \left[\frac{\partial^2 \tilde{\omega}_i^{\text{GCPA}}(\{q_i\})}{\partial q_{i,L} \partial q_{i,L'}} \right]_{\{q_i\}=\{q_i^0\}}. \quad (48)$$

The functional of Eq. (47) constitutes a generalization of the CEF proposed in Ref. 26 for discussing the charge transfers in metallic alloys and shall then be referred to in the following as the CEF. With respect to our previous work, here Eq. (47) includes not only the charge excesses $q_{i,00}$, but also the charge multipole moments with $\ell > 0$.

The minimization of the CEF functional $\tilde{\Omega}^{\text{CEF}}$ with respect to its variables, the set of the multipole moments $\{q\}$, and the chemical potential μ gives

$$\sum_{L'} [a_{i,LL'} (q_{i,L'} - q_{i,L'}^0) + M_{LL',ij} q_{j,L'}] = \mu \delta_{i,00} \quad (49)$$

and

$$\sum_i q_{i,00} = 0. \quad (50)$$

By using the definition of the Madelung potentials [Eq. (39)] and setting

$$k_{i,L} = \sum_{L'} a_{i,LL'} q_{i,L'}^0 + \mu \delta_{i,00}, \quad (51)$$

it is easy to show that Eq. (49) for $L=(0,0)$ coincides with the linear laws given by Eq. (45). Versions of Eqs. (49)–(51) with the angular momentum summations truncated at $\ell=0$ can be found in Ref. 26.

We wish to highlight that the CEF derivation from the GCPA functional is based on the assumption, common to all Ginzburg–Landau theories,^{58,59} that the homogeneously disordered phase, in the present case the random alloy phase, can be the starting point for a perturbative treatment of ordering or segregation phenomena. As discussed in the previous subsection, in the GCPA context, this amounts to conjecture that the coherent scattering-path matrix \mathcal{I}^c of a random alloy can be used for obtaining a physical picture of concentration fluctuations or, in other words, that it is able to *represent* such fluctuations.

We wish to close this section with a few comments. The principal result of this paragraph, the CEF functional of Eq. (47), has been obtained by a series expansion of the GCPA functional about the values that the multipole moments would have in the absence of coupling. The series has been terminated at the lowest order at which differences with respect to isomorphous approximations are expected for. This, not surprisingly, is enough to obtain a physical picture of the charge transfers in metallic alloys. For a given alloy configuration, the linear Euler–Lagrange equations obtained by minimizing the CEF can be easily solved for the charge multipole moments. The procedure requires the inversion of the matrix \underline{F} of elements

$$F_{ij,LL'} = a_{i,LL'} \delta_{ij} + M_{ij,LL'}. \quad (52)$$

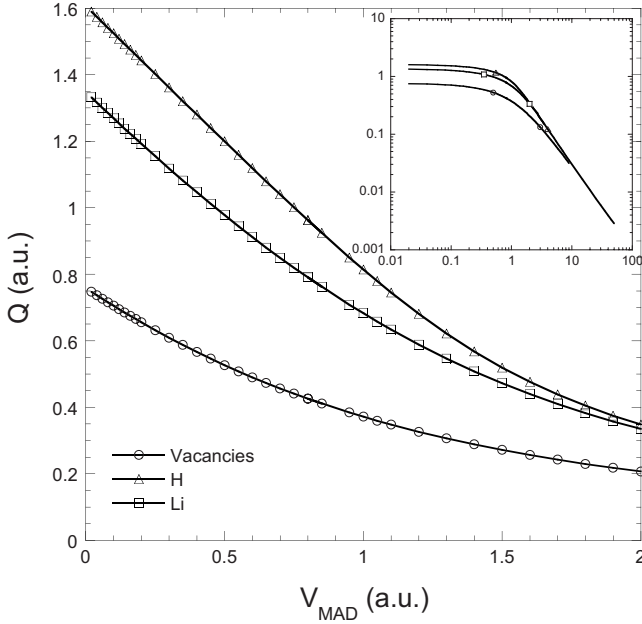


FIG. 7. qV relationships for light substitutional impurities (vacancies, H and Li atoms) dissolved in bcc Al from CPA+LF calculations. The quantity Q is the number of valence electrons at the impurity site, therefore, $Q=0$ corresponds to zero electrons for vacancies and H atoms and two electrons for Li. The linear behaviors observed for small fields ($V_{Mad} < 1$ a.u.) are superseded by power law trends (see the log-log plot in the inset) for very high fields.

As we have shown elsewhere,^{26,60} for a given alloy configuration, the value of the CEF functional at its minimum has the physical meaning of the total energy of the same configuration. The ambiguity due to the presence of the above mentioned concentration dependent constant can be resolved by comparing CEF and GCPA calculations for a single configuration in a fixed concentration ensemble.

In the previous subsection, we have described a general procedure based on the numerical integration of the qV laws for evaluating the functional form of $\tilde{\omega}_i^{GCPA}(\{q_i\})$. Of course, if the random alloy \mathcal{r}^c was able to represent concentration fluctuations and the qV laws were linear, the GCPA and the CEF functionals would be coincident. We do not think that the qV laws can be truly linear. The argument is as follows. The local excesses of electrons, $q_{i,00}$, accordingly with the physical intuition and with the results plotted in Figs. 5 and 6 are nonincreasing functions of the Madelung potential $V_{i,00}^{Mad}$. If the qV laws were really linear, $q_{i,00}$ would indefinitely decrease and eventually reach unphysical values, $q_{i,00} < Z_i$ corresponding to negative charge densities. Actually, we expect that the linear laws cannot be any longer valid when all valence electrons are expelled from the site. This circumstance would correspond to some critical value for the charge excess, say, $q_{i,00}^{crit}$. Before this critical value is reached, the qV laws should exhibit a crossover to an asymptotic behavior, say, $q_{i,00} \rightarrow q_{i,00}^{crit}$ as $V_{i,00}^{Mad} \rightarrow \infty$. We have tested this conjecture by executing CPA+LF calculations²⁵ for single impurities (vacancies, H or Li atoms) embedded in Al. The results are shown in Fig. 7, where we plot $Q = q_{i,00} - q_{i,00}^{crit}$ for the impurity site as a function of the relevant Madelung fields. In all the cases considered, a linear regime is clearly visible at low

fields. At very high fields, a crossover to a power law dependence is observed, with the number of electrons tending to the critical value from above. The crossover field is comparable to the host bandwidth. We recall that in CPA+LF calculations, \mathcal{r}^c is that of the host, while the Madelung potential is just an adjustable parameter. While this is a sensible way for studying the response of the impurity to the perturbing field, this does not imply that all the range of the perturbations considered is physically meaningful. We do not think that such high fields, corresponding to the tunneling regime in the impurity site, could occur in real systems as this would require a too large defect of electrons at the impurity nearest neighbors. Hence, Fig. 7, while supporting the view that the linearity of the qV laws and the CEF are just approximations, does not support the possibility that, at least for metallic systems, appreciable deviations from linearity or failures of the CEF are likely to occur.

Another point we wish to address is concerned with the value of the chemical potential μ in Eq. (47). In a recent paper, Drchal *et al.*⁶¹ argued that μ should be always zero since the Fourier transform of the Madelung coefficients with $L=L'=(0,0)$ diverges as $k \rightarrow \infty$, implying that the sum of the charge excesses $\Sigma q_{i,00}$ must vanish, automatically satisfying the electroneutrality constraint. The observation of Drchal *et al.* is correct for infinite systems, while for finite supercells, even with periodic boundary condition, the same Fourier transform always remains finite. k , in fact, can take only the values of the reciprocal space vectors that constitute the tiling of the supercell considered.⁵¹ The set of the allowed values for k includes 0 only for infinitely large supercells. In most practical calculations, μ is necessary, although it usually takes small nonzero values.

IV. NUMERICAL RESULTS

In this section, we present a series of numerical tests designed to study the limits of validity of the GCPA and CEF theoretical frameworks. The central issues here shall be in investigating the realm of validity of the linear qV laws [Eq. (45) or (49)] and of the energetics implied by the CEF functional [Eq. (47)]. Furthermore, we shall try to answer two questions: (i) to what extent the CEF is able to approximate GCPA calculations and (ii) how do the predictions from the CEF and the GCPA compare vs exact DFT calculations for ordered systems. The GCPA theory chosen for these tests is the PCPA⁴³ that, being based on a supercell approach, allows for easy comparison vs exact DFT calculations.

Several kinds of *ab initio* parameter-free calculations shall be presented in this section. The “exact” DFT results used for comparison shall be the LDA full-potential LAPW calculations produced by using the WIEN2 *ab initio* package.^{29,62} They are referred below as LAPW. In all the cases, about 10^4 k points in the full Brillouin zone have been used, the spherical harmonics expansion of the potentials in the muffin-tin spheres has been truncated at $\ell=6$, and the parameter $R_{MT}K_{Max}$ has been set to 7. The PCPA calculations have been performed by a conveniently modified version of our KKR-CPA code.⁶³ They are based on the ASA approximation for the site potentials and, accordingly with the discussion in

TABLE I. CEF parameters obtained by the linear regression of the qV data from PCPA calculations for random $\text{Cu}_c\text{Zn}_{1-c}$ alloys in bcc or fcc lattices. C_{Cu} and C_{Zn} are defined as the difference between 1 and the correlations obtained from the regressions for the Cu and Zn site charges; r is given by the ratio $(k_{\text{Cu}}-k_{\text{Zn}})(a_{\text{Cu}}a_{\text{Zn}})^{-1/2}$. All the quantities are expressed in a.u. CEF calculations using the coefficients presented in this table are referred to as CEF-PCPA.

	c	a_{Cu}	a_{Zn}	$k_{\text{Cu}}-k_{\text{Zn}}$	C_{Cu}	C_{Zn}	r
	0.20	1.223	1.211	0.146	3×10^{-7}	1×10^{-6}	0.120
	0.25	1.225	1.214	0.147	4×10^{-7}	1×10^{-6}	0.121
	0.33	1.223	1.215	0.148	5×10^{-7}	2×10^{-6}	0.121
bcc	0.50	1.219	1.214	0.146	5×10^{-7}	2×10^{-6}	0.120
	0.67	1.215	1.214	0.144	3×10^{-7}	2×10^{-6}	0.119
	0.75	1.214	1.214	0.144	3×10^{-7}	2×10^{-6}	0.119
	0.80	1.213	1.214	0.144	3×10^{-7}	9×10^{-7}	0.119
	0.20	1.220	1.212	0.138	3×10^{-7}	1×10^{-6}	0.113
	0.25	1.221	1.214	0.140	3×10^{-7}	9×10^{-7}	0.115
	0.33	1.222	1.216	0.142	3×10^{-7}	1×10^{-6}	0.116
fcc	0.50	1.222	1.217	0.143	5×10^{-7}	2×10^{-6}	0.117
	0.67	1.223	1.222	0.145	5×10^{-7}	1×10^{-6}	0.119
	0.75	1.222	1.223	0.145	3×10^{-7}	1×10^{-6}	0.119
	0.80	1.222	1.222	0.145	3×10^{-7}	2×10^{-6}	0.119

Sec. II B, equal atomic volumes are used for all lattice sites. Our calculations use several thousand k points in the full Brillouin zone and 31 energies over a complex Gaussian integration contour. For both LAPW and PCPA calculations, the core electron treatment is fully relativistic, while a non-relativistic approximation is used for valence states. Finally, we present CEF calculations^{26,64} with the charge multipolar expansion truncated at $\ell=0$. The concentration dependent parameters required by the CEF have been obtained from the linear regressions of the qV data generated from supercells with random occupancies and the required mean atomic concentrations and are reported in Tables I and II. Depending on which was the source of the parameters, the CEF calculations shall be referred to as CEF-PCPA or CEF-LAPW. By using the formalism of the previous section, for both PCPA and CEF calculations, we set $w_i=1$ for all lattice sites, $\lambda_{00}=1$, and $\lambda_{\ell m}=0$ for $\ell > 0$.

A. qV laws

In Sec. III, we have presented the CEF functional as an approximation for the GCPA functional and have shown how this is equivalent to assume the linearity of the qV laws. In Figs. 5 and 6, we plot the qV curves from our PCPA calculations for the binary bcc $\text{Cu}_{0.50}\text{Zn}_{0.50}$ and the quaternary $\text{Al}_{0.25}\text{Cu}_{0.25}\text{Ni}_{0.25}\text{Zn}_{0.25}$ fcc random alloys. It is surprising to observe how accurately the PCPA data can be fitted by straight lines. The correlation coefficients obtained from the linear regression of the same data differ from unit by about 10^{-6} . Similar very high correlations are always obtained

TABLE II. CEF parameters obtained by the linear regression of the qV data from LAPW calculations for random $\text{Cu}_c\text{Zn}_{1-c}$ alloys in bcc or fcc lattices. C_{Cu} and C_{Zn} are defined as the difference between 1 and the correlations obtained from the regressions for the Cu and Zn site charges; r is given by the ratio $(k_{\text{Cu}}-k_{\text{Zn}})(a_{\text{Cu}}a_{\text{Zn}})^{-1/2}$. All the quantities are expressed in a.u. CEF calculations using the coefficients presented in this table are referred to as CEF-LAPW.

	c	a_{Cu}	a_{Zn}	$k_{\text{Cu}}-k_{\text{Zn}}$	C_{Cu}	C_{Zn}	r
	0.25	2.968	2.181	0.456	3×10^{-2}	2×10^{-2}	0.179
	0.33	2.704	2.327	0.445	4×10^{-3}	8×10^{-3}	0.177
bcc	0.50	2.811	2.307	0.413	9×10^{-3}	5×10^{-2}	0.162
	0.67	3.388	3.351	0.590	3×10^{-3}	7×10^{-3}	0.175
	0.75	2.586	2.652	0.432	3×10^{-2}	1×10^{-2}	0.165
	0.25	2.457	1.949	0.360	5×10^{-3}	9×10^{-4}	0.165
fcc	0.50	2.287	2.130	0.350	9×10^{-3}	3×10^{-3}	0.159
	0.75	2.646	2.317	0.399	4×10^{-3}	2×10^{-4}	0.161

from the analysis of PCPA qV data, as it is evident by looking at Table I. As shown in Table II, also LAPW data present high correlations, although the corresponding linear fits are not perfect and their correlations deviate from unit by 10^{-2} or 10^{-3} . This notwithstanding, as argued in Sec. III C, we believe that the linearity of the qV relationships within the PCPA is just an approximation. In order to check out how accurate it is, we have studied one of the most difficult realistic cases, that of a high charge transfer ordered alloy, namely, the CuZn system. This system has been studied with many different theoretical approaches.⁶⁵⁻⁷⁰ It is also relevant, for our present concerns, that the total energy differences between fcc and bcc geometrical alloy arrangements are relatively small. We have executed calculations for all the set of 62 bcc- and fcc-based structures reported in Refs. 30 and 31. These structures include several ordered crystals for each of the following Cu atomic concentrations: 0.20, 0.25, 0.33, 0.50, 0.66, 0.75, and 0.80. In order to facilitate the comparison, the lattice constants have been kept fixed to the values 5.5 and 6.9 a.u., respectively, for bcc- and fcc-based lattices. The results for bcc- and fcc-based alloys are reported in Tables III and IV, respectively.

The charges from the CEF-PCPA are, in practice, identical to those obtained from the PCPA theory for the ordered systems. In order to represent the size of these tiny differences, we report in Tables III and IV the mean square displacement between the two sets of calculated charges, $\langle(\Delta q)^2\rangle$. In the worst case, the bcc-based DO_2 structure, identified in Table IV by 86, we find $\langle(\Delta q)^2\rangle=6 \times 10^{-8}$. Such an excellent agreement has been obtained for all the set of ordered structures considered, in spite of the fact that the CEF input has been obtained from random supercells.

In a previous Letter,²⁶ we have shown that the CEF is able to carefully reproduce the charges from locally self-consistent multiple scattering (LSMS) calculations. Moreover, the parameters extracted from ordered structure calculations can be used to predict the charges for random

TABLE III. Charge excesses and total energies per atom for bcc-based $\text{Cu}_c\text{Zn}_{1-c}$ alloys. The first two columns on the left give, for each system, the mean Cu atomic concentration (c) and, when available, the supercell identifier in the database of Ref. 31 (conf). “R” followed by a number, e.g., R16, stands for a quasirandom supercell containing the corresponding number of atoms not included in the database. In the third column, n^{unl} indicates the mean number of unlike nearest neighbors of Zn sites. Columns 4–7 report the MSD of the charge excesses, $\langle(\Delta q)^2\rangle$, obtained by the comparison of different theories: (a) PCPA vs CEF-PCPA, (b) LAPW vs CEF-PCPA, (c) LAPW vs CEF-LAPW, and (d) LAPW vs the model of Ref. 41. Columns 8–11: total energies per atom from PCPA, CEF-PCPA, LAPW, and CEF-LAPW calculations. The energy zero is given, for each concentration, by the PCPA prediction for the ground state.

c	conf	n^{unl}	$\langle(\Delta q)^2\rangle$				ΔE (mRy)			
			(a)	(b)	(c)	(d)	PCPA	CEF-PCPA	LAPW	CEF-LAPW
0.20	92	1.5	5×10^{-11}	1×10^{-4}			0.038	0.040	-0.015	
	98	2.0	2×10^{-9}	4×10^{-4}			0.000	0.000	0.000	
0.25	69	2.0	3×10^{-9}	4×10^{-5}	2×10^{-6}		0.741	0.742	0.991	0.556
	72	1.3	9×10^{-9}	4×10^{-4}	2×10^{-5}		1.966	1.971	3.951	2.437
	75	2.0	1×10^{-9}	1×10^{-5}	1×10^{-6}		0.824	0.823	1.089	0.631
	78	2.7	1×10^{-9}	4×10^{-4}	5×10^{-7}		0.865	0.864	0.980	0.838
	81	2.7	3×10^{-8}	2×10^{-4}	4×10^{-7}		0.353	0.353	0.050	0.246
	83	2.7	2×10^{-8}	3×10^{-4}	1×10^{-6}		0.327	0.327	0.194	0.260
	86	2.7	6×10^{-8}	4×10^{-4}	2×10^{-5}		0.000	0.000	0.000	0.000
	R16	2.2	1×10^{-8}	1×10^{-4}	3×10^{-6}		0.797	0.799	1.117	0.669
0.33	63	3.0	3×10^{-8}	2×10^{-4}	2×10^{-5}		0.000	0.000	0.000	0.000
	65	2.0	2×10^{-9}	3×10^{-4}	2×10^{-5}		1.741	1.747	2.950	2.129
	67	4.0	2×10^{-8}	2×10^{-4}	3×10^{-5}		0.078	0.078	-0.519	0.068
	R18	3.3	6×10^{-9}	3×10^{-4}	4×10^{-5}		0.558	0.562	0.729	0.838
0.50	60	4.0	4×10^{-9}	4×10^{-5}	5×10^{-6}	3×10^{-4}	1.661	1.662	3.457	1.188
	61	8.0	3×10^{-9}	1×10^{-3}	6×10^{-6}	3×10^{-3}	0.000	0.000	0.000	0.000
	71	2.0	2×10^{-9}	1×10^{-3}	4×10^{-5}	9×10^{-4}	4.107	4.115	8.657	5.089
	74	4.0	3×10^{-9}	5×10^{-7}	4×10^{-7}	3×10^{-4}	1.823	1.824	3.666	1.342
	77	4.0	4×10^{-11}	2×10^{-4}	1×10^{-6}	7×10^{-5}	2.736	2.739	4.804	2.404
	80	6.0	7×10^{-9}	4×10^{-4}	8×10^{-7}	3×10^{-4}	0.885	0.883	1.666	0.557
	85	4.0	7×10^{-9}	2×10^{-4}	1×10^{-5}	7×10^{-4}	1.007	1.006	2.757	0.646
	R16	4.3	3×10^{-9}	2×10^{-4}	3×10^{-6}	4×10^{-4}	1.989	1.989	3.806	1.613
0.67	62	6.0	7×10^{-10}	2×10^{-4}	6×10^{-7}		0.000	0.000	0.000	0.000
	64	4.0	8×10^{-12}	3×10^{-4}	2×10^{-5}		1.698	1.703	2.671	2.021
	66	8.0	2×10^{-10}	1×10^{-4}	2×10^{-7}		0.076	0.077	-0.650	0.061
	R18	6.7	3×10^{-9}	3×10^{-4}	1×10^{-6}		0.545	0.549	0.508	0.870
0.75	68	6.0	2×10^{-11}	2×10^{-5}	1×10^{-6}		0.726	0.732	1.364	0.566
	70	4.0	3×10^{-9}	6×10^{-4}	3×10^{-5}		1.927	1.935	3.395	2.505
	73	6.0	2×10^{-10}	9×10^{-6}	2×10^{-6}		0.806	0.812	1.390	0.642
	76	8.0	1×10^{-9}	5×10^{-4}	4×10^{-6}		0.850	0.852	1.022	0.873
	79	8.0	3×10^{-9}	2×10^{-4}	1×10^{-6}		0.345	0.349	0.464	0.251
	82	8.0	4×10^{-9}	3×10^{-4}	2×10^{-6}		0.322	0.323	0.462	0.269
	84	8.0	3×10^{-8}	4×10^{-4}	4×10^{-6}		0.000	0.000	0.000	0.000
	R16	6.8	1×10^{-9}	2×10^{-4}	3×10^{-6}		0.782	0.788	1.278	0.685
0.80	87	6.0	5×10^{-10}	1×10^{-4}			0.033	0.038	0.327	
	93	8.0	4×10^{-10}	6×10^{-4}			0.000	0.000	0.000	

structures and vice versa. The quality of the CEF predictions was very good too, with $\langle(\Delta q)^2\rangle$ of the order of 10^{-6} , i.e., about 3 orders of magnitude less than what we have found by

the comparison of CEF and PCPA. Since the LSMS calculations presented in Ref. 26 were based on the ASA, we surmise that the modest loss of accuracy of CEF predictions for

TABLE IV. Charge excesses and total energies per atom for fcc-based $\text{Cu}_c\text{Zn}_{1-c}$ alloys. The first two columns on the left give, for each system, the mean Cu atomic concentration (c) and, when available, the supercell identifier in the database of Ref. 31 (conf). “R” followed by a number, e.g., R16, stands for a quasirandom supercell containing the corresponding number of atoms not included in the database. In the third column, n^{unl} indicates the mean number of unlike nearest neighbors of Zn sites. Columns 4–7 report the MSD of the charge excesses, $\langle(\Delta q)^2\rangle$, obtained by the comparison of different theories: (a) PCPA vs CEF-PCPA, (b) LAPW vs CEF-PCPA, (c) LAPW vs CEF-LAPW, and (d) LAPW vs the model of Ref. 41. Columns 8–11: total energies per atom from PCPA, CEF-PCPA, LAPW, and CEF-LAPW calculations. The energy zero is given, for each concentration, by the PCPA prediction for the ground state.

c	conf	n^{unl}	$\langle(\Delta q)^2\rangle$				ΔE (mRy)			
			(a)	(b)	(c)	(d)	PCPA	CEF-PCPA	LAPW	CEF-LAPW
0.20	35	2.5	3×10^{-10}	2×10^{-5}			0.500	0.503	0.926	
	39	3.0	7×10^{-9}	7×10^{-5}			0.000	0.000	0.000	
0.25	12	3.3	2×10^{-9}	7×10^{-5}	4×10^{-6}		0.515	0.516	1.078	0.438
	15	2.7	1×10^{-8}	2×10^{-4}	4×10^{-7}		1.379	1.386	2.151	1.658
	18	3.3	2×10^{-9}	2×10^{-5}	2×10^{-6}		0.566	0.568	1.054	0.471
	21	3.3	2×10^{-9}	1×10^{-4}	8×10^{-6}		0.680	0.685	1.510	0.616
	24	4.0	2×10^{-8}	2×10^{-4}	5×10^{-6}		0.000	0.000	0.000	0.000
	26	4.0	2×10^{-8}	2×10^{-4}	3×10^{-7}		0.068	0.069	0.073	0.051
	29	2.0	5×10^{-9}	4×10^{-4}	2×10^{-5}		1.817	1.824	4.202	2.349
0.33	R16	3.0	1×10^{-8}	2×10^{-4}	1×10^{-6}		1.015	1.020	1.705	1.169
	6	4.0	1×10^{-10}	5×10^{-5}			1.179	1.185	1.016	
	8	5.0	1×10^{-8}	1×10^{-4}			0.000	0.000	0.000	
0.50	10	3.0	6×10^{-11}	3×10^{-4}			1.800	1.807	3.300	
	3	8.0	7×10^{-9}	3×10^{-4}	5×10^{-6}	1×10^{-4}	0.139	0.144	-0.075	0.111
	4	6.0	2×10^{-9}	5×10^{-6}	2×10^{-5}	6×10^{-5}	1.075	1.081	2.141	0.961
	14	4.0	1×10^{-9}	6×10^{-4}	5×10^{-6}	2×10^{-4}	2.895	2.905	4.803	3.657
	17	7.0	3×10^{-9}	3×10^{-5}	2×10^{-6}	1×10^{-6}	0.717	0.720	1.121	0.605
	20	6.0	5×10^{-10}	5×10^{-5}	1×10^{-7}	5×10^{-5}	1.429	1.434	2.464	1.353
	23	8.0	7×10^{-9}	2×10^{-4}	1×10^{-6}	4×10^{-5}	0.000	0.000	0.000	0.000
	28	3.0	2×10^{-9}	9×10^{-4}	6×10^{-5}	5×10^{-4}	3.339	3.350	6.745	4.694
0.67	R16	6.8	3×10^{-9}	2×10^{-4}	2×10^{-6}	6×10^{-5}	0.913	0.918	1.519	0.972
	5	8.0	3×10^{-10}	9×10^{-5}			1.102	1.224	1.283	
	7	10.0	1×10^{-8}	1×10^{-4}			0.000	0.000	0.000	
	9	6.0	3×10^{-9}	3×10^{-4}			1.743	1.866	3.224	
0.75	11	10.0	3×10^{-10}	9×10^{-5}	2×10^{-5}		0.549	0.550	1.009	0.501
	13	8.0	5×10^{-9}	5×10^{-4}	3×10^{-6}		1.479	1.482	2.230	1.986
	16	10.0	3×10^{-10}	2×10^{-5}	1×10^{-5}		0.604	0.605	1.054	0.535
	19	10.0	5×10^{-10}	1×10^{-4}	5×10^{-6}		0.729	0.731	1.083	0.709
	22	12.0	3×10^{-9}	2×10^{-4}	5×10^{-6}		0.000	0.000	0.000	0.000
	25	12.0	2×10^{-9}	2×10^{-4}	5×10^{-6}		0.073	0.073	-0.193	0.057
0.80	27	6.0	1×10^{-8}	5×10^{-4}	1×10^{-5}		1.944	1.949	3.654	2.799
	R16	3.0	2×10^{-9}	3×10^{-4}	2×10^{-6}		1.088	1.091	1.790	1.409
	30	10.0	1×10^{-9}	6×10^{-5}			0.544	0.550	-4.023	
	36	12.0	2×10^{-8}	7×10^{-5}			0.000	0.000	0.000	

LSMS with respect to PCPA calculations constitutes a measure of the importance of the scattering effects from nearest neighbors. These effects, in fact, can be accounted for only in a mean field fashion by the PCPA.

We have also investigated the effects of the spherical approximation for the atomic potentials by executing full-potential LAPW calculations. In Fig. 8, we plot the site charge excesses obtained from LAPW vs the number of un-

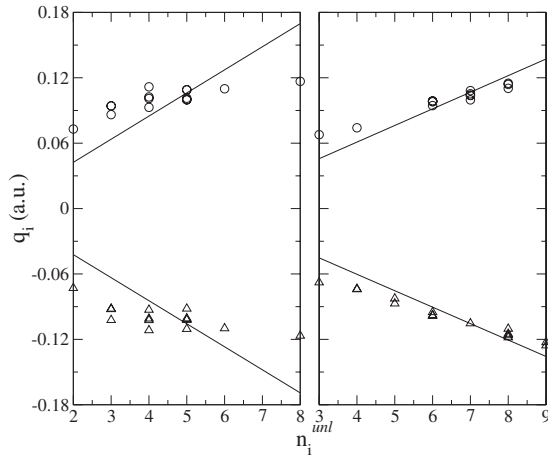


FIG. 8. Charge excesses q_i vs the number of unlike nearest neighbors of the corresponding site, n_i^{unl} , from LAPW calculations for many, bcc- and fcc-based, ordered and disordered, configurations of $\text{Cu}_{0.50}\text{Zn}_{0.50}$ alloys. Circles and triangles represent charges on Cu and Zn sites, respectively. Left frame: bcc-based alloys; right frame: fcc-based alloys. The straight lines in each panel indicate the best fits obtained by the model of Magri *et al.* (Ref. 41).

like nearest neighbors of the same sites, for all the structures corresponding to equimolar concentrations. In Tables III and IV, we report the results for $\langle(\Delta q)^2\rangle$ at all the concentrations. As apparent from Fig. 8, the trends of q_i are not easily accounted for by the nearest neighbor environment only,⁴¹ especially for bcc-based structures. This notwithstanding, CEF-PCPA calculations reasonably account for the LAPW charges. As can be seen in the columns marked as (b) in Tables III and IV, $\langle(\Delta q)^2\rangle$ is usually of the order of 10^{-4} , sometimes less, and about 10^{-3} in the worst case. In order to understand how much these results can be affected by the PCPA input coefficients, we have repeated CEF calculations by fitting the coefficients from the LAPW qV data for the random alloy configurations corresponding to the relevant stoichiometries and reported in Tables III and IV. As shown in column (c) of Tables III and IV, this reduces $\langle(\Delta q)^2\rangle$ of about 1 order of magnitude.

Interestingly, the present CEF-LAPW calculations confirm the observations about the transferability of CEF parameters in Ref. 26, where the CEF charges have been compared to the LSMS results. As a typical example, let us consider the results for $c=0.50$ reported in Table III. The $\langle\Delta q^2\rangle$ obtained are always small: 4×10^{-5} in the worst case and 4×10^{-7} in the best, corresponding, respectively, to structures 71 and 74, while an intermediate value 3×10^{-6} is found for structure R16, from which the CEF-LAPW coefficients have been obtained. The same holds for all the concentrations, both for bcc and fcc structures. A look to column (c) in the Tables III and IV, in fact, shows that excellent results have been obtained for all the supercells, and that, very often, the agreement obtained for the random structure from which the CEF coefficients have been extracted is not necessarily the best.

The above arguments about the charges should not lead to the conclusion that, for this purpose, any fit is comparable to any other. This is clearly shown in Fig. 9, where the performances of PCPA, CEF-PCPA, CEF-LAPW, and by the

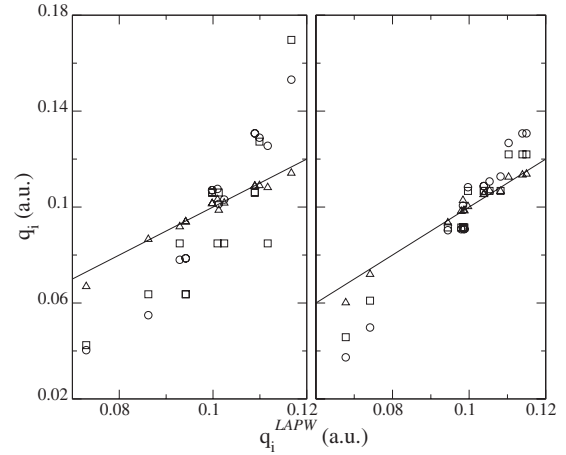


FIG. 9. Charge excesses on Cu sites q_i for the same $\text{Cu}_{0.50}\text{Zn}_{0.50}$ alloys as in Fig. 8. Circles, triangles, and squares represent the calculated values by CEF-PCPA, CEF-LAPW, and by the model of Ref. 41. In the abscissa, the charge excesses obtained by LAPW calculations are reported. Left frame: bcc-based alloys; right frame: fcc-based alloys. In order to improve readability, we also plot the straight lines $q=q^{LAPW}$. The deviations from these lines measure the accuracy of the various calculations.

model of Magri *et al.*⁴¹ are compared for the equiatomic concentration alloys. In the same figure, the distances from the diagonal lines measure the differences between the LAPW charges and those by various approximations for all the Cu sites in the supercells with $c=0.5$. It is there evident that the results by CEF-LAPW, marked by open triangles, are much better than those by other approximations.

A comment is due about the sets of CEF coefficients, the a 's and the k 's, obtained by the best fit of the qV laws from PCPA and LAPW and reported in Tables I and II. At first sight, it seems that the large discrepancies between the two sets could not be explained by the different approximations used by the two methods. It should be noticed, however, that for the systems considered, the \underline{F} matrix of Eq. (52) is dominated by its diagonal elements, the a 's. Under these circumstances, as it can be argued along the lines of Ref. 60 by taking the appropriate limit, the charge transfers are almost completely determined by the ratios $r=(k_A-k_B)/a$, where a is the geometrical mean of a_A and a_B . As seen in Tables I and II, the differences between r_{PCPA} and r_{LAPW} are much smaller.

B. Total energies

In Tables III and IV, we compare the total energies obtained for CuZn alloys by CEF, PCPA, and LAPW calculations. We have used the same extended set of bcc- and fcc-based structures listed in Ref. 31. Since the CEF energies contain a concentration dependent constant, we report the quantity ΔE defined as the energy difference between the structure at hand and the structure that, at the same concentration, has the lowest energy, according to PCPA calculations. The same ΔE is plotted in Figs. 10 and 11 for the Cu concentrations $c=0.25, 0.50$, and 0.75 , for which the data-

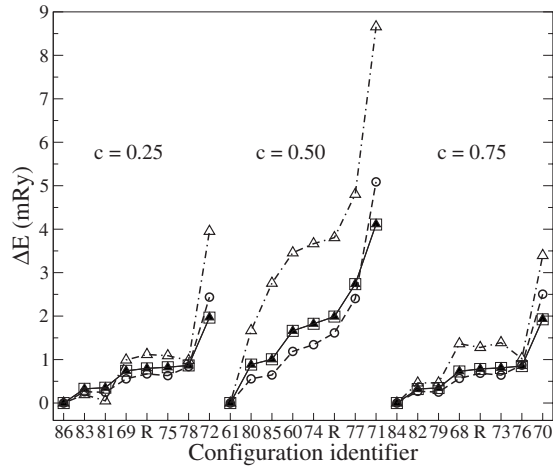


FIG. 10. Total energy differences with respect to the PCPA predicted ground state, ΔE , for bcc-based $\text{Cu}_c\text{Zn}_{1-c}$ alloys. The labels indicated in the abscissa identify the various configurations in the database of Ref. 31; R stands for structures with randomly generated chemical occupations containing 16 atoms with mean Cu contents $c=0.25$, 0.5, and 0.75. Open triangles, open circles, open squares, and filled triangles indicate LAPW, CEF-LAPW, CEF-PCPA, and PCPA calculations, respectively. Lines are a guide for the eyes.

base of Ref. 31 contains a number of structure sufficient to individuate trends.

Our first observation is that the total energies obtained by PCPA and CEF-PCPA calculations perfectly overlap on the scale of Figs. 10 and 11, where they are represented as filled triangles and open squares, respectively. As reported in Tables III and IV, in fact, the values obtained by the two methods are different by a few μRy per atom, which is com-

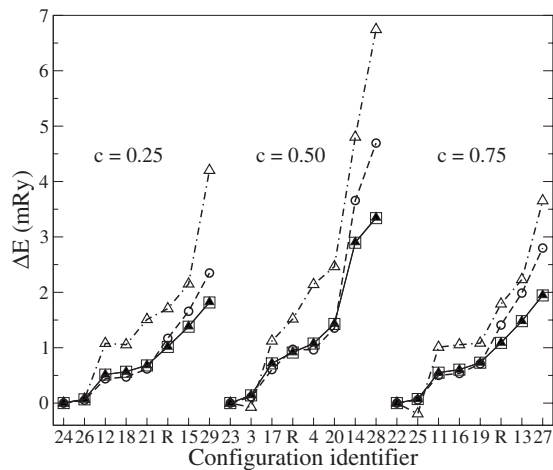


FIG. 11. Total energy differences with respect to the PCPA predicted ground state, ΔE , for fcc-based $\text{Cu}_c\text{Zn}_{1-c}$ alloys. The labels indicated in the abscissa identify the various configurations in the database of Ref. 31; R stands for structures with randomly generated chemical occupations containing 16 atoms with mean Cu contents $c=0.25$, 0.5, and 0.75. Open triangles, open circles, open squares, and filled triangles indicate LAPW, CEF-LAPW, CEF-PCPA, and PCPA calculations, respectively. Lines are a guide for the eyes.

parable to the accuracy of the calculations. Thus, PCPA and CEF-PCPA give indistinguishable results both for the charges (as discussed in the previous subsection) and the total energies. Therefore, it is compelling to conclude that the CEF theory is a numerically excellent and powerful tool to reproduce with much less efforts GCPA electronic structure calculations. Moreover, since CEF-PCPA calculations use as an input the qV data obtained from *random* supercells, the perfect agreement obtained for the properties of so many different *ordered* structures that have not been used to fit the CEF coefficients has only one possible explanation. Accordingly, with the discussion in Secs. III B and III C, both the following conditions must be fulfilled. (i) The coherent scattering-path matrix $\underline{\tau}^c$ of the random alloy configuration used as an input must be representative of the whole set of ordered structures considered; (ii) the linearity of the qV laws is almost perfectly observed in all the range of values that the charge excesses and the Madelung potentials take for the structures considered. In Sec. III, we have offered several arguments supporting the validity of both points above, but we have not been able to provide an analytical demonstration. We think that the numerical evidence found is very strong and compelling.

Accordingly with the discussion in Sec. III, the success of the CEF theory in reproducing the charges or, equivalently, the Madelung potentials guarantees the reproducibility of *any* ground state property within the GCPA theory through Eq. (41). Hence, even spectral properties as the DOS or the Bloch spectral functions, although buried, are contained in the CEF functional that, if the input parameters are extracted from a GCPA theory, inherits all the good and the bad things of same GCPA theory.

The comparison with LAPW calculations is more difficult for two different reasons. In the first place, these calculations do not assume mean boundary conditions for the wave functions and use a procedure equivalent to the full calculation of the $\underline{\tau}$ matrix. In the second place, within LAPW calculations, the charge multipole summation is truncated at some high ℓ value. With these clarifications, the agreement between LAPW and PCPA or CEF-PCPA calculations (there is no reason for discussing the last two models separately) is quite good. As a general rule, the two sets of calculations find the same ground states at the concentrations considered. In the few exceptions (that correspond to the negative figures in the LAPW columns of Tables III and IV), the disagreement can be explained by the fact that the structures indicated as the ground state by the two theories are almost degenerate in energy. Also, the general trends for the total energies are well reproduced, as seen in Figs. 10 and 11, though the PCPA generally underestimates the energy differences.

Fitting the CEF parameters from the LAPW qV laws generally improves the agreement. At variance of what is found for the charges, however, the improvement is quite modest.

In summary, the CEF appears able to perfectly reproduce GCPA calculations for both ordered and disordered metallic systems. The reasons why the agreement is so excellent are not yet completely understood. Although CEF and GCPA theories are both coarse-grained versions of the DFT, opposite to what numerical results suggest, they are not the *same* theory. In fact, as discussed in Sec. III, in order to be coin-

cident to the CEF, GCPA theories should (i) exactly observe linear qV laws and (ii) lead to coherent scattering matrices independent of the configuration in a fixed concentration ensemble. For metallic alloys, these conditions appear plausible and the numerical evidence strongly supports the view that both are nearly satisfied. However, we must highlight that condition (i) is not verified for pathologically high values of the Madelung field. The comparison vs LAPW calculations suggest that both coarse-grained theories, GCPA and CEF, are able to semiquantitatively reproduce the total energies of the alloy configurations considered. In particular, the results by the coarse grained theories are strongly correlated with those by LAPW. This fact is better elucidated in Figs. 10 and 11, where configurations belonging to the same fixed concentration ensemble are ordered in such a way to have increasing PCPA total energies. If the same ordering was not observed by some other method for some configuration, this would show up as a local minimum in the corresponding curve. The most visible of such events occurs in Fig. 11 for $c=0.75$, where the curve corresponding to LAPW calculations presents a very weak local minimum at configuration 25. The examination of Figs. 10 and 11 suggests that the coarse-grained theories are able to qualitatively give correct predictions about ordering for the alloys considered, while the fact that they generally underestimate the corresponding energies could imply incorrect estimates of the corresponding transition temperatures.

V. CONCLUSIONS

We wish to conclude this paper with a summary and a few comments. We have introduced the class of the GCPA theories that are characterized by (i) a specific ansatz for the kinetic part of the density functional, which is common to all CPA-based theories, and (ii) an external model that determines the way in which the atomic effective potentials should be reconstructed and the statistical weights to be assigned each. The GCPA class of approximations includes most existing CPA-based density functional theories, to mention a few, the CPA prototype, i.e., the isomorphous CPA,^{22,32} SIM-CPA,^{44,45} the PCPA,⁴³ the CPA+LF,²⁵ and the nonlocal CPA.⁵⁰ The ansatz (i) consists in applying averaged boundary conditions at the surfaces of each scattering volume and naturally leads to algorithms requiring a number of operation that scales as N . As discussed by Abrikosov and Johansson,⁴⁰ CPA-based approximations allow for a careful picture of the spectral properties of metallic alloys. The so much criticized results of the isomorphous CPA about the total alloy energies can be healed by external models that consider the charge distribution in the system. We have shown how this can be systematically done by writing the relevant energetic contributions as a series involving the charge multipole moments in each scattering volume. The truncation errors of the same series are probably already quite small when only the first term is included, as in the case of spherical approximations.

We have derived an expression of the GCPA density functional that, together with the above multipole sums, includes

local atomic terms completely determined by the atomic number of the ion in the volume and by the geometry of the same volume. The local term at the i th site is coupled to the others only through the coherent scattering matrix \mathcal{T}^c and the Madelung potential at the same site. Although this kind of coupling, which we have called marginal coupling, is not necessarily weak, nevertheless, it is analytically tractable and it is the source of the $O(N)$ scaling in GCPA theories. We have demonstrated that in a GCPA theory, all ground state properties within a specific sample are functions of the appropriate coupling Madelung potential only or, equivalently, of the charge multipole moments at each lattice site. To put it into other words, we have demonstrated that the GCPA approximations realize a *coarse graining* of the Hohenberg–Kohn density functional since only a part of the information conveyed by the electronic density field, namely, the charge multipole moments, actually enters in the GCPA approximate functional. Moreover, we have suggested that the explicit form of the GCPA functional dependence on the multipole moments can be obtained in a fixed concentration ensemble by the numerical integration of the qV relationships for a random alloy configuration belonging to the same ensemble. The above procedure does not rely on the linearity of the qV laws.

We have rederived the CEF²⁶ as a sensible approximation of the GCPA theories, with which it would coincide provided that the qV were exactly linear as claimed by many groups. The present derivation allows for the inclusion of higher order multipole moments. A very remarkable feature of the CEF theory is that it shares the same structure of the MST. In fact, the minimization of the CEF requires the solution of a set of Euler–Lagrange equation that has the same structure of the Korringa–Kohn–Rostoker (KKR) matrix at zero energy and wave vector.^{60,61} More specifically, as can be seen by comparing Eqs. (4) and (5), the site-diagonal response functions $a_{i,LL'}$ and the Madelung coefficients $M_{ij,LL'}$ in the CEF theory play the role of the site-diagonal scattering matrices and the KKR structure constants in the MST theory. The correspondence is not only formal since the $a_{i,LL'}$ are single-site quantities in the same sense of the single-site scattering matrices⁶⁰ and, in plain analogy with them, are related to the single-site response to the appropriate perturbing field.²⁵

In the present paper, we have provided several formal arguments and strong numerical evidences that CEF and GCPA theories lead to very similar results, the discrepancies being of the order of the numerical errors. We have also shown that CEF and GCPA theories are able to reproduce the charges and the total energies for many ordered alloy configurations. In our view, the *coarse-grained theories*, GCPA and CEF, constitute a valuable alternative to full DFT calculations.

Although the CPA theory was proposed many years ago with the purpose of dealing with substitutionally disordered alloys, we think that we have shown that, today, GCPA theories are able to deal with ordered intermetallic compounds too. Therefore, the fact that CPA-based theories are able to cope with sophisticated model of disorder is not an original sin but rather an added value.

The computational performances of the CEF have been discussed in more detail elsewhere.²⁶ Here, we like to mention that the possibility of evaluating total energies for thousand atoms in a few second CPU time could constitute a substantial enlargement of the domain of the applications of the DFT.

ACKNOWLEDGMENTS

We acknowledge financial support from MURST (PRIN Grant No. 2004023079/004). Discussions with L. Zingales, B. Ginatempo, and I. A. Abrikosov are also gratefully acknowledged.

*ebruno@unime.it

- ¹P. Hohenberg and W. Kohn, Phys. Rev. **136**, B864 (1964).
- ²N. D. Mermin, Phys. Rev. **137**, A1441 (1965).
- ³*Density Functional Methods in Physics*, edited by R. M. Dreizler and J. da Providencia (Plenum, New York, 1985).
- ⁴*Density Functional Theory*, edited by E. K. U. Gross and R. M. Dreizler (Plenum, New York, 1995).
- ⁵R. M. Dreizler and E. K. U. Gross, *Density Functional Theory* (Springer-Verlag, Berlin, 1990).
- ⁶A. Gonis, *Green Functions for Ordered and Disordered Systems* (North-Holland, Amsterdam, 1992).
- ⁷R. Car and M. Parrinello, Phys. Rev. Lett. **55**, 2471 (1985).
- ⁸W. Kohn and L. J. Sham, Phys. Rev. **140**, A1133 (1965).
- ⁹W. Yang, Phys. Rev. Lett. **66**, 1438 (1991).
- ¹⁰P. Cortona, Phys. Rev. B **44**, 8454 (1991).
- ¹¹F. R. Krajewski and M. Parrinello, Phys. Rev. B **71**, 233105 (2005).
- ¹²J. Harris, Phys. Rev. B **31**, 1770 (1985).
- ¹³S. Goedecker, Rev. Mod. Phys. **71**, 1085 (1999).
- ¹⁴J. Koringa, Physica (Amsterdam) **13**, 392 (1947).
- ¹⁵W. Kohn and N. Rostoker, Phys. Rev. **94**, 1111 (1953).
- ¹⁶Y. Wang, G. M. Stocks, W. A. Shelton, D. M. C. Nicholson, Z. Szotek, and W. M. Temmerman, Phys. Rev. Lett. **75**, 2867 (1995).
- ¹⁷I. A. Abrikosov, A. M. N. Niklasson, S. I. Simak, B. Johansson, A. V. Ruban, and H. L. Skriver, Phys. Rev. Lett. **76**, 4203 (1996).
- ¹⁸R. Zeller, P. H. Dederichs, B. Ujfalussy, L. Szunyogh, and P. Weinberger, Phys. Rev. B **52**, 8807 (1995).
- ¹⁹P. J. Braspenning and A. Lodder, Phys. Rev. B **49**, 10222 (1994).
- ²⁰P. Soven, Phys. Rev. **156**, 809 (1967).
- ²¹G. M. Stocks, W. M. Temmerman, and B. L. Gyorffy, Phys. Rev. Lett. **41**, 339 (1978).
- ²²D. D. Johnson, D. M. Nicholson, F. J. Pinski, B. L. Gyorffy, and G. M. Stocks, Phys. Rev. Lett. **56**, 2088 (1986).
- ²³J. S. Faulkner, Y. Wang, and G. M. Stocks, Phys. Rev. B **52**, 17106 (1995).
- ²⁴J. S. Faulkner, Y. Wang, and G. M. Stocks, Phys. Rev. B **55**, 7492 (1997).
- ²⁵E. Bruno, L. Zingales, and A. Milici, Phys. Rev. B **66**, 245107 (2002).
- ²⁶E. Bruno, L. Zingales, and Y. Wang, Phys. Rev. Lett. **91**, 166401 (2003).
- ²⁷L. Pauling, *The Nature of the Chemical Bond* (Cornell University Press, Ithaca, NY, 1960).
- ²⁸O. K. Andersen, Phys. Rev. B **12**, 3060 (1975).
- ²⁹K. Schwarz, P. Blaha, and G. Madsen, Comput. Phys. Commun. **147**, 71 (2002).
- ³⁰S. Curtarolo, D. Morgan, and G. Ceder, CALPHAD: Comput. Coupling Phase Diagrams Thermochem. **29**, 163 (2005).
- ³¹S. Curtarolo, Ph.D. thesis, MIT, 2003.
- ³²D. D. Johnson, D. M. Nicholson, F. J. Pinski, B. L. Gyorffy, and G. M. Stocks, Phys. Rev. B **41**, 9701 (1990).
- ³³P. Lloyd, Proc. Phys. Soc. London **90**, 207 (1967).
- ³⁴J. S. Faulkner, J. Phys. C **10**, 4661 (1977).
- ³⁵B. L. Gyorffy and M. J. Stott, *Band Structure Spectroscopy of Metals and Alloys* (Academic, London, 1972).
- ³⁶J. F. Janak, Phys. Rev. B **9**, 3985 (1974).
- ³⁷E. U. Condon and G. Shortley, *The Theory of Atomic Spectra* (Cambridge University Press, Cambridge, 1951), Vol. II.
- ³⁸J. S. Faulkner and G. M. Stocks, Phys. Rev. B **21**, 3222 (1980).
- ³⁹J. S. Faulkner, Prog. Mater. Sci. **27**, 1 (1982).
- ⁴⁰I. A. Abrikosov and B. Johansson, Phys. Rev. B **57**, 14164 (1998).
- ⁴¹R. Magri, S. H. Wei, and A. Zunger, Phys. Rev. B **42**, 11388 (1990).
- ⁴²J. S. Faulkner, N. Y. Moghadam, Y. Wang, and G. M. Stocks, Phys. Rev. B **57**, 7653 (1998).
- ⁴³B. Ujfalussy, J. S. Faulkner, N. Y. Moghadam, G. M. Stocks, and Y. Wang, Phys. Rev. B **61**, 12005 (2000).
- ⁴⁴I. A. Abrikosov, Y. H. Vekilov, and A. V. Ruban, Phys. Lett. A **154**, 407 (1991).
- ⁴⁵I. A. Abrikosov, Y. H. Vekilov, P. A. Korzhavyi, A. V. Ruban, and L. E. Shilkrot, Solid State Commun. **83**, 867 (1992).
- ⁴⁶D. D. Johnson and F. J. Pinski, Phys. Rev. B **48**, 11553 (1993).
- ⁴⁷S. Faulkner, J. S. Pella, A. Rusanu, Y. Puzlyev, T. Leventouri, G. M. Stocks, and B. Ujfalussy, Philos. Mag. **86**, 2661 (2006).
- ⁴⁸J. S. Faulkner, B. Ujfalussy, N. Moghadam, G. M. Stocks, and Y. Wang, J. Phys.: Condens. Matter **13**, 8573 (2001).
- ⁴⁹S. Pella, J. S. Faulkner, G. M. Stocks, and B. Ujfalussy, Phys. Rev. B **70**, 064203 (2004).
- ⁵⁰D. A. Rowlands, J. B. Staunton, and B. L. Gyorffy, Phys. Rev. B **67**, 115109 (2003).
- ⁵¹D. A. Rowlands, J. B. Staunton, B. L. Gyorffy, E. Bruno, and B. Ginatempo, Phys. Rev. B **72**, 045101 (2005).
- ⁵²F. Mammano, E. Bruno, and N. Fiorino (unpublished).
- ⁵³E. H. Lieb, Int. J. Quantum Chem. **24**, 243 (1983).
- ⁵⁴H. Englisch and R. Englisch, Phys. Status Solidi B **123**, 711 (1984).
- ⁵⁵J. S. Faulkner, B. Ujfalussy, N. Moghadam, G. M. Stocks, and Y. Wang, J. Phys.: Condens. Matter **13**, 8573 (2001).
- ⁵⁶W. Kohn, Phys. Rev. Lett. **76**, 3168 (1996).
- ⁵⁷E. Bruno, B. Ginatempo, E. S. Giuliano, A. V. Ruban, and Y. K. Vekilov, Phys. Rep. **249**, 353 (1994).
- ⁵⁸A. G. Khachatryan, *Theory of Structural Transformations in Solids* (Wiley, New York, 1983).
- ⁵⁹*First Principles Theories of Disordered Alloys and Alloy Phase*

- Stability*, edited by P. E. A. Turchi and A. Gonis (Plenum, New York, 1994).
- ⁶⁰E. Bruno, *Mater. Sci. Eng., A* **462**, 456 (2007).
- ⁶¹V. Drchal, R. Hammerling, and P. Weinberger, *Phys. Rev. B* **74**, 214202 (2006).
- ⁶²P. Blaha, K. Schwarz, G. Madsen, D. Kvasnicka, and J. Luitz, *WIEN2k, An Augmented Plane Wave Plus Local Orbitals Program for Calculating Crystal Properties* (Vienna University of Technology, Vienna, 2001).
- ⁶³E. Bruno and B. Ginatempo, *Phys. Rev. B* **55**, 12946 (1997).
- ⁶⁴E. Bruno and L. Zingales, *Philos. Mag.* **84**, 1621 (2004).
- ⁶⁵J. D. Althoff, D. D. Johnson, F. J. Pinski, and J. B. Staunton, *Phys. Rev. B* **53**, 10610 (1996).
- ⁶⁶V. Crisan, H. Ebert, P. Entel, and H. Akai, *Comput. Mater. Sci.* **17**, 151 (2000).
- ⁶⁷S. Muller and A. Zunger, *Phys. Rev. B* **63**, 094204 (2001).
- ⁶⁸D. A. Rowlands, A. Ernst, B. L. Gyorffy, and J. B. Staunton, *Phys. Rev. B* **73**, 165122 (2006).
- ⁶⁹K. Tarafder, A. Chakrabarti, K. K. Saha, and A. Mookerjee, *Phys. Rev. B* **74**, 144204 (2006).
- ⁷⁰P. R. Tulip, J. B. Staunton, D. A. Rowlands, B. L. Gyorffy, E. Bruno, and B. Ginatempo, *Phys. Rev. B* **73**, 205109 (2006).
- ⁷¹Matrices in the angular momentum space are denoted by a single underline; double underline is used for matrices both in the angular momentum and in the site spaces. Angular momentum components are denoted by capital letters, $L \equiv (\ell, m)$, $L' \equiv (\ell', m')$, ..., and site components by small Latin letters, i, j, \dots .
- ⁷²In the present paper, the convention is used that for any function of the position, $f_i(\mathbf{r})$ stands for $f(\mathbf{r}-\mathbf{R}_i)$ with $\mathbf{r} \in v_i$.
- ⁷³In our notation $\{V_i^{Mad}\}$ stands for the set of all the Madelung coefficients of the i th site, and $\{V_{i,L_1}^{Mad}, V_{i,L_2}^{Mad}, \dots\}$ and $\{V^{Mad}\}$ for the set of all the Madelung coefficients at all crystal sites, i.e., $\{V^{Mad}\} = \{V_{i_1}^{Mad}\} \cup \{V_{i_2}^{Mad}\} \cup \dots$. The notations $\{q_i\}$ and $\{q\}$ have a similar meaning.